Effects of ocean acidification on acid-base physiology, skeleton properties, and metal contamination in two echinoderms from vent sites in Deception Island, Antarctica

Di Giglio S.[1], Agüera A.[1,2], Pernet Ph.[1], M'Zoudi S.[1], Angulo-Preckler C.[3], Avila C.[4], Dubois Ph.[1]

1. Laboratoire de Biologie Marine, Université Libre de Bruxelles, CP 160/15, Avenue F.D. Roosevelt 50, 1050 Bruxelles, Belgium

2. Institute of Marine Research in Norway, Austevoll Research Station, Sauganeset 16, 5392 Norway

3. Norwegian College of Fishery Science, Faculty of Biosciences, Fisheries and Economics, UiT The Arctic University of Norway, Tromsø, Norway

4. Department of Evolutionary Biology, Ecology and Environmental Sciences, Faculty of Biology and Biodiversity Research Institute (IRBio), Universitat de Barcelona, Av. Diagonal 643, 08028 Barcelona, Catalonia.

KEY WORDS: West Antarctic Peninsula (WAP), echinoderms, calcification, marine benthic invertebrates, mechanical properties, metals contamination, ocean acidification

1. Abstract

Antarctic surface waters are expected to be the first to experience severe ocean acidification (OA) with carbonate undersaturation and large decreases in pH forecasted before the end of this century. Due to the long stability in environmental conditions and the relatively low daily and seasonal variations to which they are exposed, Antarctic marine organisms, especially those with a supposedly poor machinery to eliminate CO_2 and protons and with a heavily calcified skeleton like echinoderms, are hypothesized as highly vulnerable to these environmental shifts. The opportunities offered by the natural pH gradient generated by vent activities in Deception Island caldera, Western Antarctic Peninsula, were used to investigate for the first time the acid-base physiologies, the impact of OA on the skeleton and the impact of pH on metal accumulation in the Antarctic sea star *Odontaster validus* and sea urchin *Sterechinus neumayeri*. The two species were sampled in four stations within the caldera, two at pH (total scale) 8.0- 8.1 and two at reduced pH 7.8. Measured variables were pH, alkalinity, and dissolved inorganic carbon of the coelomic fluid; characteristic fracture force, stress and Young's modulus using Weibull statistics and Cd, Cu, Fe, Pb and Zn concentrations in the integument, gonads and digestive system. Recorded acid-base characteristics of both studied species fit in the general picture deduced from temperate and tropical sea stars and sea urchins but conditions and possibly confounding factors, principally food availability and quality, in the studied stations prevented definitive conclusions. Reduced seawater pH 7.8 and metals had almost no impact on the skeleton mechanical properties of the two investigated species despite very high Cd concentrations in *O. validus* integument. Reduced pH was correlated to increased contamination by most metals but this relation was weak. Translocation and caging experiments taking into account food parameters are proposed to better understand future processes linked to ocean acidification and metal contamination in Antarctic echinoderms.

2. <u>Introduction</u>

Human activities are the principal causes of the increasing emissions of global atmospheric carbon dioxide (CO_2) (Andersson *et al.*, 2005; Burns, 2008; Tyrrell, 2011). Atmospheric CO_2 concentration raised from a preindustrial value of 280 ppm to 413 ppm today (August 2020, Ed

Dlugokencky and Pieter Tans, NOAA/ESRL (https://www.esrl.noaa.gov/gmd/ccgg/trends/)). This CO_2 contributes to global warming although 25-30 % are taken up by the oceans (Sabine *et al.*, 2004, Solomon *et al.*, 2008). The ocean absorption of atmospheric CO_2 leads to shifts in the dissolved inorganic carbon (DIC) equilibrium: when the seawater pCO_2 increases (hypercapnia), the pH and carbonate ion concentration decrease (acidosis). By the end of the 21st century, with an expected atmospheric pCO_2 of 485 to 900 ppm, the seawater pH could decrease by up to 0.3-0.4 units (IPCC, 2014; Jewett and Romanou, 2017; Marsh, 2008) and the horizons of saturation of calcium carbonates will locally shoal to the surface (Feely *et al.*, 2004). These modifications are known as ocean acidification (OA) (Caldeira and Wickett, 2003). In turn, these changes in the carbonate system lead to shifts in metal speciation and bioavailability in seawater (Millero et al., 2009).

Surface waters of the Antarctic zone of the Southern Ocean (>60° S) are particularly exposed to these changes because the solubility of CO_2 increases with decreasing temperatures and the Antarctic upwelling brings CO_2 rich water to the surface. Therefore, naturally higher CO_2 and lower carbonate ion concentrations have been already recorded in the Antarctic zone (Monteiro et al., 2020; Sabine et al., 2004). Consequently, Antarctic surface waters are expected to be the first to experience carbonate undersaturation and large decreases in pH (McNeil and Matear, 2008; Steinacher and Joos, 2016). Furthermore, some Antarctic regions are among the most affected by global warming, like the West Antarctic Peninsula (WAP) which is the most rapidly warming region in the Southern hemisphere (IPCC, 2014; Turner et al., 2014, Massom and Stammerjohn, 2010; Montes-Hugo et al., 2009).

Due to the long stability in environmental conditions, including temperature and pH, and the relatively low daily and seasonal variations to which they are exposed, Antarctic marine taxa are hypothesized as vulnerable to environmental shifts, particularly in temperature and pH (Orr *et al.*, 2005; Peck, 2005). Echinoderms include numerous species which play significant ecological roles in the carbon cycling and diversity of the Antarctic macrobenthos (Angulo-Preckler et al., 2018, 2017b; Arntz and Gallardo, 1994; Gutt et al., 1998; Morse et al., 2019; Rogers et al., 2019). Antarctic adult echinoderms were hypothesized to be particularly vulnerable to OA due to their low metabolism - associated to a supposed poor machinery to eliminate CO_2 and protons - and heavily calcified high-magnesium calcite skeleton (McClintock *et al.*, 2011; Sewell and Hofmann, 2011). However, the few available studies on Antarctic echinoderms reported contrasted responses and indicated that they might be more tolerant than expected, at least at the adult stage (Ingels *et al.*, 2012; Constable *et al.*, 2014; Peck, 2018). Under OA, Antarctic sea urchins larvae have been shown to be resilient until pH_{SW} 7.6 (Byrne et al., 2013; Ericson et al., 2010; Foo et al., 2016; Kapsenberg and Hofmann, 2014). On the contrary, the sea star *Odontaster validus* showed negative responses to OA at the larval stage with lower survival and delay of developmental steps (Gonzalez-Bernat et al., 2012). Antarctic adult sea urchins were reported to have the same acid-base characteristics as temperate and tropical species (Collard *et al.*, 2015). Although Dell'Acqua *et al.*, (2019) reported a significant effect on the reproductive condition of the sea urchin *Sterechinus neumayeri* after a short term experiment, a similar decrease of 0.5 pH units for 24 or 40 months had no effect on the energetics and gonad or test growth of the same species (Suckling *et al.*, 2015; Morley *et al.*, 2016). Currently, no data is available on the acid-base response to OA or on the effects of this on the skeleton of Antarctic echinoderms, which is considered at risk by many authors (McClintock *et al.*, 2011; Sewell and Hofmann, 2011; Duquette *et al.*, 2018).

Shallow hydrothermal vents offer an interesting opportunity to assess the life-long impact of OA by providing gradients of pH established for a long time. These have been extensively used during the last decade in temperate and tropical regions (*e.g.* Hall-Spencer *et al.*, 2008; Fabricius *et al.*, 2011; Kroeker *et al.*, 2012; Linares *et al.*, 2015; Di Giglio *et al.*, 2020b). Because some of these vents also emit metals, they also allow assessing the impact of OA on metal accumulation by organisms (Bray et al., 2014). To our knowledge, no vent site has been investigated as a surrogate to global change effects in the Southern Ocean. Port Foster, the submerged caldera of Deception Island, South Shetland Islands (WAP), which shows several hydrothermal vents, might be such a site. The presence of several vents could also allow the deconvolution of the effects of temperature, pH, and metals, because different gradients are present (Angulo-Preckler et al., 2018; Deheyn et al., 2005; Guerra et al., 2011; Kusakabe et al., 2009; Somoza et al., 2004). Although environmental conditions of Deception Island might seem hostile for marine life to settle (Berrocoso et al., 2018; Flexas et al., 2017) and despite the fact that the island has undergone periodic eruption events throughout its history (Rey et al., 1995), the marine community from Port Foster is rich. It is mainly composed by opportunistic species (bivalves, annelids, amphipods) with the macro-epibenthic fauna strongly represented by key echinoderm species such as *Ophionotus victoriae*, *Odontaster validus* and *Sterechinus neumayeri* in very high abundances (Lovell and Trego, 2003; Barnes et al., 2008; Angulo-Preckler et al., 2017a, 2017b, 2018).

The present study used the opportunities offered by the vent activities in Deception Island caldera to address the following questions: (1) is the acid-base physiological answer to acidification of Antarctic echinoderms similar to that of temperate and tropical species; (2) is the skeleton of Antarctic echinoderms affected by acidification as predicted; (3) is metal accumulation by Antarctic echinoderms affected by acidification. We investigated these questions in the two dominant epibenthic echinoderms in the caldera, the sea urchin *S. neumayeri* and the sea star *O. validus*.

3. Materials and Methods

3.1. Sampling

Organisms, water and sediment were collected by scuba diving within four stations of Port Foster inside the caldera of Deception Island, South Shetland Islands, West Antarctic Peninsula at the end of February 2018 (Fig. 1). The stations were the same as those described in Angulo-Preckler *et al.* (2018). Samples were collected at 15 m depth, where temperature and salinity of the seawater were the most stable. Six sea stars *O. validus* Koehler 1906 and six sea urchins *S. neumayeri* (Meissner 1900) were collected alongside with three seawater samples (50 mL) and three sediment samples (500g, top 2-cm layer) per station. Individuals were maintained in 30 L tanks filled with aerated seawater collected at the same station and immediately brought back to the laboratory and analysed.

Directly after sampling, the physico-chemical characteristics (salinity, temperature, pH and alkalinity) of seawater were measured. Besides, 3 mL seawater were stored in a gas-tight glass tube (Exetainer 3mL) at 4°C with 0.5 µL of $HgCl_2$ (7%) for further measurement of dissolved inorganic carbon concentration (DIC). Sediments were dried in a stove (50°C for one night) and a part studied as a total fraction. The sediment was stored dried for further metal analysis. All individuals of each species were weighted (wet weight) and measured with a calliper. Also, 3.5 to 6.0 mL of the fluid of the coelomic cavity (= coelomic fluid = CF) was extracted by puncture of the oral membrane with a syringe and a needle. A part of the extracted CF (500µL) was used to measure the pH while the remaining CF was centrifuged (2000g for 3 minutes) at 4°C and stored with 3µL $HgCl_2$ (7%) to avoid other biological activity, for further analysis of DIC. Then, organisms were dissected and the gonads, the integument and the pyloric caeca separated for sea stars; and gonads, integument and digestive tract (emptied of its content) for sea urchins. All the compartments were weighted, dried in an oven at 50°C for at least 24 h and stored until subsequent analysis of metals or mechanical testing of the skeleton.

3.2. Physico-chemical measurements in seawater and in the coelomic fluid (CF)

All measurements took place in an unheated external lab at Deception Island and samples were maintained on ice when measured. The seawater electromotive force (e.m.f.) was measured using a pH-meter (Metrohm 826 pH mobile) with a combined glass electrode (Metrohm 6.0228.010), while the CF e.m.f. was obtained using a microelectrode (same pH meter, combined with glass electrode Metrohm 6.0224.100). All measured e.m.f. were then converted to total scale pH according to DelValls and Dickson (1998) method with the calibration based on Tris/AMP buffers. Total alkalinity (TA) of seawater was measured by titration using Gran's function as described in Collard et al. (2013b). To measure the DIC, the samples (CF and seawater) were prepared following the method described in Di Giglio *et al.* (2020b): 1 µL of phosphoric acid (99%) was deposited on the bottom of a 3 mL empty Exetainer tube. After the latter tube was flushed with helium for 2 min, 250 µL of the sample were transferred from the sampling tube to the flushed tube using a gas tight syringe. The tubes were stirred for 12 h before analysis. Samples of CO_2 were taken by an automatic sampler (Conflo IV universal continuous flow interface) and analysed in an isotope-ratio mass spectrometer (IRMS, nu instrument) (Gillikin et al., 2010). Parallel to the tubes containing samples of seawater and coelomic fluid, tubes with $NaHCO_3$ solutions of known concentrations were also measured. These known DIC concentrations were plotted vs. area of the total signal peak of CO_2 detected by the mass spectrometer in order to obtain a calibration curve for DIC in the samples. Analysis of the certified reference material provided by Dickson (batch #151) was within 5.4% of the certified value.

Aragonite and calcite saturation states (Ω) as well as pCO_2 and the concentrations of the carbonate system components in the sea water and these parameters together with TA in the CF were calculated from DIC, pH (total scale), salinity and temperature data (measured in the laboratory and corrected with the field data) using the software CO_2SYS (Pierrot et al., 2006) with the dissociation constants for carbonate from Mehrbach *et al.* (1973) refitted by (Dickson and Millero (1987), and for KSO_4 from Dickson (1990).

3.3. Metal analyses

Sediment samples (total fraction) and the different compartments from the two species (integument, gonads and pyloric caeca for the sea stars and integument, digestive tract and gonads for the sea urchins) were weighted and a subsample of *ca.* 0.25g was oven dried (48 h; 60°C) at Deception Island. Further experiments took place at the lab of Marine biology at the Université Libre de Bruxelles. Dried sediment samples were placed in acid-washed Teflon vials with Suprapure hydrogen peroxide (H_2O_2) 65% and Suprapure nitric acid 30% (HNO_3) (Sutherland, 2002). Samples were mineralized in a micro-wave oven (MILESTONE 1200 mega) using increasing power (250w, 400w, 600w and 800w) – 6 min each. All digested samples were filtered under vacuum on a glass microfiber (Whatman GF/A, retention 1.6 µm, 25 mm diameter) and diluted in MilliQ water to 50 ml. Concentrations of Pb, Cu and Cd were analysed by graphite furnace atomic absorption spectrometry (Varian GTA-100 SpectrAA 6402Z). Concentrations of Zn and Fe were measured by atomic flame absorption spectrometry (GBC 906 AA spectrophotometer). A certified material (278R Community Bureau of Reference Certified Material) mussel soft-tissue powder was analysed with the experimental samples to check the accuracy of the methodology. Analyses of the certified reference material were always within 8.2 % of the certified value.

3.4. Ossicle sampling and preparation for mechanical tests

The oven-dried integument of the six sea stars and the six sea urchins per station were cleaned of soft tissues by soaking them into a NaOCl 2.5% solution for 60 min, rinsed with Supra-pure (Sartorius) water and then further soaked in a NaOCl 5.25% solution for 30 min and rinsed with Suprapur water (Sartorius). The solutions were always stirred to prevent the formation of lactic acid and corrosion of the ossicles. The ossicles were air-dried for at least 24 h before their use. The absence of corrosion on plates after the cleaning was checked by observation in a scanning electron microscope (JEOL JSM-7200).

From each individual, five ambulacral plates, *i.e.* the tube feet holding plates, near the mouth of the sea stars, and five interambulacral ambital plates, *i.e.* the largest plates of the test, of the sea urchins were sampled. In total, 30 ossicles of each type per species per station were submitted to mechanical tests.

All mechanical tests performed were carried out at room temperature (18 °C). As both types of plates are considered as beams (length is at least ten times the height), we used a three-point bending test, which was carried out as described in Moureaux *et al.*, (2011) and Collard *et al.* (2016), respectively for sea stars and sea urchins.

Each ossicle was first photographed sideways in front of millimetre paper in order to measure the effective length (length in between the two supporting points) and the thickness of the plates using the Image J software (Schneider *et al.*, 2012, Rasband, W.S., U. S. National Institutes of Health, Bethesda, Maryland, USA). They were then placed on a metal stand and the mechanical test was performed using a non-cutting blade fixed on the loading device. It was lowered on the middle of the ambulacral plate and on the primary tubercle of ambital plates at a speed of 0.05 mm min^{-1} until fracture. One of the two halves of the fractured plates was mounted on an aluminium stub coated with gold and its fracture surface was imaged under scanning electron microscope (JEOL JSM-7200). The second moment of area (I_2) was measured using the macro MomentMacro (developed by Ruff C., Johns Hopkins University School of Medicine, MD, USA) in the software ImageJ (Schneider *et al.*, 2012, Rasband,W.S., U.S.National Institutes of Health, Bethesda,MD, USA). I_2 (m^4) is a description of the geometric distribution of material around a neutral plane of bending and reflects the proportion of stereom in the plate fracture surface (vs. pores).

$$I_2 = \int y^2 \, dA \quad (1)$$

Where y: the distance to the neutral plane of bending (m) and A: the area (m^2).

The apparent Young's modulus, E (Pa), characterizing the material stiffness, was calculated according to the linear-elastic beam theory:

$$E = \frac{F_{max} \, L_e^3}{48 \, \Delta L \, I_2} \quad (2)$$

Where: F_{max}: force at fracture (N), ΔL: displacement (m), L_e: effective length (m) and I_2: second moment of area (m^4).

The flexural stress of the ossicle in a beam under three-point bending was calculated with:

$$\sigma = E \, . \, \varepsilon = \frac{F_{max} \, L_e^2}{48 \, I_2} \quad (3)$$

Where σ: the bending stress at fracture (Pa), E, Young's modulus (Pa), ε, the strain (=ΔL/L, dimensionless), F_{max}: force at fracture (N), L_e: effective length (m) and I_2: second moment of area (m^4).

3.5. Statistical analyses

All ANOVA models and GLM models were built according to the recommendations of Doncaster and Davey (2007) and followed by Tukey test using the appropriate mean square error for multiple comparisons when ANOVA p-value was < 0.05.

Physico-chemical parameters of seawater, CF and metals concentration (in the total fraction of the sediments) were analysed with one factor ANOVA (station: fixed factor) for each species separately. Relations between metal concentrations in the different organism compartments and pH in the CF (pH_{CF}) were analyzed by canonical correlation analysis. Relationships between contamination (with metals concentration at each station) for all compartments and pH_{CF} were also analyzed with principal-component analysis (PCA). Significance of PCA-resulting groups (=stations) was determined using one factor ANOVA on PCA scores of the first and second principal components (PC) separately, and pairwise comparisons were performed using Tukey's test.

Relationships between size (L_e and H) and mechanical properties (F_{max}, I_2 and ΔL) were tested with simple Pearson correlations before performing ANOVAs. L_e was compared according to station using model III ANOVA (station: fixed factor, individual: random factor nested in station). Relations between mechanical properties, pH_{CF} and metal concentrations in the integument were analysed by GLM using as the final model:

Considered mechanical variable = a[Cd] + b[Pb] + c[Cu] + d[Fe] +e [Zn] + f pH_{CF} + g [Cd]* pH_{CF} + h [Pb]* pH_{CF} + i [Cu]* pH_{CF} + j [Fe]* pH_{CF} + k [Zn]* pH_{CF} + constant (4)

3.6. Weibull analysis

Mechanical properties (F_{max}, Young's modulus (E) and stress (σ)) were analysed using Weibull distribution (the cumulative probability function):

$$P_{f\,i} = 1 - \exp\left(-\left(\frac{\sigma_i}{\sigma_0}\right)^m\right) \qquad (5)$$

Where P_f is the probability of failure that increases with the stress variable, σ (Pa). Weibull modulus, m (dimensionless), corresponds to the distribution of flaws within the specimen and the homogeneity of their distribution increased with m. The characteristic stress σ_0 is an experimentally obtained parameter that corresponds to a proportion of fractured samples of (1 – 1/e) = 63% (cumulative failure probability). In this study, the characteristic values of the ossicles of each species has been compared according to the stations by using the 95% confidence intervals (CI 95) with the modified least square regression of Bütikofer et al. (2015) and following the methods described by Di Giglio et al. (2020a) .

4. Results

Detailed statistical results are presented as supplementary information (Tables S01 to S15).

4.1. Seawater physico-chemical parameters and metal concentrations in the sediment

Temperature did not differ between the studied stations. Mean seawater pH_T ranged between 7.77 and 8.13 (Table 1, S01). BAE and WHB, considered as control stations, showed the highest pH_T whereas BID and TEL stations had a significantly lower pH ($p_{ANOVA} < 10^{-3}$ $p_{Tukey} \leq 0.023$). Consistently, pCO_2 at BID and TEL was significantly higher than at BAE and WHB stations ($p_{ANOVA} < 10^{-3}$, $p_{Tukey} < 10^{-3}$). Mean TA_{SW} ranged between 2298 and 2839 µmol kg^{-1} (Table 1). TA_{SW} was significantly higher at TEL than at the other stations ($p_{ANOVA} = 0.028$, $p_{Tukey} \leq 0.041$), where TA_{SW} of other stations did not significantly differ ($p_{Tukey} \geq 0.073$). DIC from TEL was significantly higher than that of BAE and BID but not of WHB ($p_{ANOVA} = 0.005$, $p_{Tukey} \leq 0.034$). The concentration in bicarbonate ions differed between the stations ($p_{ANOVA} = 0.005$) and followed the same trend as DIC. The concentration in carbonate ions (CO_3^{2-}) significantly differed between the stations ($p_{ANOVA} < 10^{-3}$), being the highest at WHB ($p_{Tukey} \leq 0.013$) and the lowest at BID and TEL ($p_{Tukey} \leq 0.041$). WHB was characterized by the highest Ω_{Ca} and Ω_{Ar}

(3.41 and 2.14 respectively, $p_{ANOVA} < 10^{-3}$, $p_{Tukey} \leq 0.013$). Values of Ω_{Ca} and Ω_{Ar} at BAE and TEL were not significantly different ($p_{Tukey} \geq 0.157$). Also, Ω_{Ca} and Ω_{Ar} at TEL and BID were not significantly different ($p_{Tukey} \geq 0.777$) but BID was characterized by significantly lower Ω_{Ca} and Ω_{Ar} than those at WHB and BAE ($p_{Tukey} \leq 0.042$).

Metals concentration (Cd, Cu, Fe, Pb and Zn) in the sediment were the highest at WHB (Table 2). The concentrations of Fe and Zn were significantly higher in this station than in all others ($p_{ANOVA} \leq 0.08$, $p_{Tukey} \leq 0.022$, Table 2, S02). TEL was systematically the station that presented the smallest concentrations in metals. The Pb concentration in WHB sediment was significantly higher than that in BAE and BID sediments ($p_{Tukey} \leq 0.036$). Cd concentrations in sediment only differed between WHB and TEL.

The relation between seawater pH and metals concentration in the sediment was tested by principal-component analysis (S03, S04). PC1 explained 73.9% of variance and metal concentrations contributed equally to this PC (~17% each metal with 21.3% for Zn), while PC2 explained 11.1% of variance and pH of seawater contributed the most to this PC (55.6%). Stations differed according to PC1 and PC2 ($p_{ANOVA} < 10^{-3}$) with WHB being significantly different from the other stations according to PC1 and from BID and TEL according to PC2 (p_{Tukey} 0.018). Seawater pH appeared poorly linked to metal concentrations in the sediment.

4.2. Acid-base physiology of the coelomic fluid (CF) and size of *O. validus* and *S. neumayeri*

Sea stars from WHB had significantly longer arms than those of TEL (Table 3, S05, p_{ANOVA} = 0.031, $p_{Tukey} \leq 0.038$). Nevertheless, mean $pH_{T\text{-}CF}$ of *O. validus* was not correlated with the length of the arm of the collected specimens ($p_{Bonferroni}$=0.288) and did not significantly differ between organisms from different stations (p_{ANOVA} =0.080) ranging between 7.65 and 7.77.

Similarly, TA, DIC, pCO_2 and bicarbonate ion concentrations of the CF did not differ between sea stars from the four stations ($p_{ANOVA} \geq 0.064$, S03). However, carbonate ion concentration and consequently Ω_{Ca} and Ω_{Ar} measured in the CF of *O. validus* were significantly different between stations ($p_{ANOVA} \leq 0.005$). Sea stars from BID showed significantly lower carbonate ion concentrations, ΩCa, and Ω_{Ar} than those from WHB and TEL but not from those of BAE. Sea stars from BAE, WHB and TEL did not differ for these variables.

Sea urchins height and diameter did not differ significantly between stations ($p_{ANOVA} \geq 0.151$,Table 3, S06) and were not significantly correlated with the pH of the CF ($p_{Bonferroni} \geq 0.263$). Mean $pH_{T\text{-}CF}$ of *S. neumayeri* from BID and TEL were significantly lower than those from sea urchins from WHB but not BAE ($p_{ANOVA} = 0.003$, $p_{Tukey} \leq 0.008$). TA of sea urchins from WHB was significantly higher than TA of sea urchins from BAE but not from BID and TEL ($p_{ANOVA} = 0.003$, $p_{Tukey\ BAE\text{-}WHB} = 0.022$, $p_{Tukey\ others} \geq 0.315$). DIC measures in the CF of sea urchins from BAE was the lowest and was significantly different from that of sea urchins from WHB and TEL ($p_{ANOVA} = 0.015$, $p_{Tukey} \leq 0.026$). ANOVA on pCO_2 measured in the CF of sea urchins was significant, however Tukey tests did not highlight any significant differences ($p_{ANOVA} = 0.035$, $p_{Tukey} \geq 0.057$). The concentration in bicarbonate ions of the CF of sea urchins from BAE was significantly lower than that of sea urchins from WHB and TEL (p_{ANOVA} = 0.005, $p_{Tukey} \leq 0.033$). The concentration in carbonate ions as well as Ω_{Ca} and Ω_{Ar} in the CF of sea urchins from WHB were significantly higher than in the other stations ($p_{ANOVA} < 10^{-3}$, $p_{Tukey} \leq 0.007$).

4.3. Morphometry and mechanical properties of the skeleton

4.3.1. *Odontaster validus* ambulacral plates

The effective length of the tested plates was not significantly different between sea stars from the different stations (Table 4, S07, $p_{ANOVA} = 0.204$). However, plates of sea stars from BID were thicker than those from sea stars of TEL ($p_{ANOVA} = 0.013$, $p_{Tukey} = 0.022$). The force at fracture (F_{max}) of the ambulacral plates was not correlated with neither arm length of the sea star nor the length or height of the plate ($p_{Bonferroni} \geq 0.184$). The second moment of area (I_2) was significantly lower in plates of sea stars from BAE than in those from BID ($p_{ANOVA} = 0.038$, $p_{Tukey} \leq 0.037$). Characteristic stress (σ_0) obtained by Weibull analyses of ambulacral plates from sea stars of BID were significantly lower than those calculated for sea stars of WHB but not from those obtained for sea stars of BAE, both control stations (Table 5, Fig. 2, S08). The characteristic force at fracture (F_{max0}) was significantly the highest in sea stars from WHB and the lowest in those from BID, with values in TEL and BAE sea stars being intermediate. The characteristic Young's modulus (E_0) of ambulacral plates was significantly lower in sea stars from BID compared to BAE and intermediate in WHB and TEL sea stars. The Weibull moduli did not differ according to station (Table 5, Fig. 3, S08).

4.3.2. *Sterechinus neumayeri* ambital plates

No morphometrical properties of the ambital plates differed according to stations ($p_{ANOVA} \geq 0.070$, Table 5, S09). There was no significant correlation between the height or the diameter of the test and the F_{max} of the ambital plates ($p_{Bonferroni} \geq 0.380$). The length and the height of the ambital plates were not significantly correlated with their F_{max} ($p_{Bonferroni} \geq 0.503$). The characteristic force at fracture (F_{max0}) of ambital plates of sea urchins was significantly lower in ambital plates of sea urchins from TEL compared to those of the two control stations (Table 5, Fig. 2, S10). The same variable did not differ in sea urchins from BID compared to those from the control stations. Other mechanical properties of ambital plates compared with Weibull statistics, *i.e.* the characteristic stress (σ_0), the characteristic Young's modulus (E_0) and the Weibull moduli (m) were not significantly different between sea urchins from control and lower pH_{SW} stations (Table 5, Fig. 2, S08).

4.4. Metals concentration in three compartments of *O. validus* and *S. neumayeri*

In both species, metal concentrations and their rankings differed according to compartments and stations (Table 6). In *O. validus*, metal concentrations in the integument of BID sea stars departed from those of other stations, showing more positive loadings along PC2 to which Cd, Cu and Pb mainly contributed (S11 A-B, S12). Metal concentrations in the gonads and pyloric caeca of WHB sea stars departed from those of the other stations, showing more negative loadings along PC1, a dimension to which all metals contributed (S11, C-F, S12). In *S. neumayeri*, metal concentrations in the integument and digestive tract of sea urchins from all stations are clearly discriminated (S12, S13A,B,E,F). Metal concentrations in the gonads of WHB sea urchins departed from those of the other stations, showing more positive loadings along PC1, a dimension to which Zn and Cu principally contributed (S12, S13C,D).

It is noteworthy that Cd concentrations in all body parts of *O. validus* were particularly high, ranging between 8.96 and 170.85 $\mu g\ g^{-1}_{DW}$, while this is not the case for *S. neumayeri* in the same stations. In both species, Fe concentrations were rather high, reaching 9652 $\mu g\ g^{-1}_{DW}$ in the former pyloric caeca and 6261 $\mu g\ g^{-1}_{DW}$ in the latter digestive tract. On the contrary, Pb concentrations in all body parts of both species are rather low, being always below 1 $\mu g\ g^{-1}_{DW}$.

In *O. validus*, concentrations of Cu, Fe and Pb in the integument were significantly negatively correlated to the pH_{T-CF} while Cd concentrations were significantly positively correlated with pH_{CF} (Table 7, S14). Correlation of Zn concentrations with pH_{CF} was not significant. In gonads, only Cd concentrations were significantly (negatively) correlated with pH_{CF}. No metal concentration in pyloric caeca were significantly correlated with pH_{CF}.

In *S. neumayeri*, concentrations of all metals in the integument were significantly negatively correlated to the pH_{CF} (Table 7, S15). In gonads, Pb and Zn concentrations were significantly negatively correlated with pH_{CF} while Cu concentrations were positively correlated with pH_{CF}. No metal concentration in the digestive tract was significantly correlated with pH_{CF}. It is noteworthy that most correlation coefficients were rather low.

4.5. Relationships between pH_{CF}, metal concentrations in the integument and mechanical properties of the skeleton

Relationships between pH_{CF}, metal concentrations in the integument and mechanical properties (F_{max}, I_2, E and stress, Table 7, S14 and S15) of the skeleton were analysed using GLM. In *O. validus*, neither stress nor Young's modulus were linked to any metal concentration or pH_{CF} (p_{Model}= 0.61 and 0.36, respectively). The model was significant for F_{max} (p_{Model}= 0.004, R^2= 0.135) although no slope of an individual factor was significant. The model was also significant for I_2 (p_{Model}= 0.004, R^2= 0.140), with the slopes for variables "Cd concentration" (negative slope) and "Cd concentration * pH_{T-CF}" (positive slope) being marginally significant ($p_{coefficient}$= 0.047). This indicates that high Cd concentrations resulted in a smaller I_2, indicating thinner or more porous plates. In *S. neumayeri*, no mechanical variable was linked to any metal concentration or to pH_{CF} (p_{Model}= 0.52, 0.60, 0.20 for, respectively stress, E, and F_{max}).

5. Discussion

5.1. Sampling stations

Seawater temperature was similar in the different stations and close to open ocean values, indicating that hot vents do not influence it on a larger scale than from the places where they are occurring. Two stations were characterized by high seawater pH_T (WHB 8.13 and BAE 8.04) and two by reduced sea water pH_T (TEL 7.82 and BID 7.77). These values are point data and a longer monitoring would be desirable. However, they correspond to those recorded in 2017 (one year before the present study) in the same stations by Angulo-Preckler *et al.* (2018). This suggests rather stable seawater acid-base conditions, at least at the time scale of echinoderm physiology. Because the Base Antártica Gabriel de Castilla is only operated 4 month a year and risk of ice scouring prevents the deployment of an autonomous pH recorder, obtaining year round pH data is currently impossible. Metal concentrations measured in the total fraction of the superficial sediment were lower than those measured previously in the sediment of several stations at Deception Island (Somoza *et al.*, 2004; Deheyn *et al.*, 2005; Guerra *et al.*, 2011). This could be linked to the much shallower location of our samples, compared to previous studies. Indeed, Deheyn *et al.* (2005) showed that metal concentration in sediments are lower away from the axis of the caldera. This is probably linked to differences in sediment origin between our shallow samples and the deeper samples of previous studies (Sturz et al., 2003) . Metal concentrations in sediment appeared poorly linked to water acidification. WHB, which has the highest pH_{SW}, was the most contaminated station while the three other stations showed lower metal concentrations in their sediment. Anyway, the metal concentrations measured in the sediment of WHB remained moderate compared to those measured in sediments of urbanized coasts of the Mediterranean and the North Sea (see *e.g.*Coteur *et al.*, 2003, Bonnano *et al.*, 2018) or of other Antarctic sites (Webb et al., 2020).

5.2. Acid-base physiology of *Odontaster validus* and *Sterechinus neumayeri*

The acid-base physiology of both species was here investigated for the first time. Samplings were carried out end of February, which means that all collected individuals of both species were in post-spawning stage (*O. validus* spawn from June to September and *S. neumayeri* from October to December; Pearse, 1991). This increased the homogeneity of the samplings but also reduced a possible effect of active gametogenesis on the acid-base physiology, like high protein concentration in the coelomic fluid. The sea star *O. validus* did not show differences in its acid-base variables between control and acidified stations except for a lower carbonate ion concentration in BID. Although sea stars from WHB were significantly larger than that of TEL, this did not influence their acid-base characteristics. Temperate sea stars studied so far do not compensate their coelomic fluid pH (pH_{CF}) when facing OA in laboratory experiments up to six months (Hernroth *et al.*, 2011; Appelhans *et al.*, 2012; Dupont & Thorndyke, 2012; Collard *et al.*, 2013a). However, Collard *et al.* (2013a) showed that the pH_{CF} of small *Asterias rubens* submitted to pH_{SW} 7.7 did not differ significantly from that of specimens maintained at control $pH_{T\text{-}SW}$ 7.9. According to these authors, this was linked to the higher surface/volume ratio of small sea stars, allowing an easier elimination of respiratory CO_2. Antarctic species have a lower metabolism when compared to tropical and temperate species (Hughes *et al.*, 2011; Peck, 2018), resulting in a lower respiratory rate in *O. validus* than in *A. rubens* (Peck *et al.*, 2008; Suszczewski *et al.*, 2010; Appelhans *et al.*, 2012, 2014; Collard *et al.*, 2013a). Indeed, the calculated $pCO_{2\text{-}CF}$ of *O. validus* (1050-1200 µatm) was lower than that of *A. rubens* (~1500-2000 µatm; Appelhans *et al.*, 2012). Therefore, we suggest that the flat morphology of *O. validus*, resulting in a lower surface/volume ratio than sea stars studied so far and a consequently easier diffusion of CO_2, together with a low oxygen consumption at temperature around 1°C, explained the similar pH_{CF} in control and acidified sites. We hypothesize that a more severe acidification would result in a decreased pH_{CF} as observed in temperate sea star. We cannot rule out a selection or adaptation of *O.validus* populations in the caldera to hypercapnic conditions but taking into account the very long pelagic larval development of this species (*ca.* half a year; Shilling and Manahan, 1994; Agüera *et al.*, 2015) and the subsequent high gene flow between populations, this is rather unlikely.

The sea urchin *S. neumayeri* showed a lower pH_{CF} in acidified stations compared to WHB. This was not linked to a size effect, as specimens from the different stations did not significantly differ for this variable. The lower pH_{CF} recorded in acidified stations is surprising as most euechinoids were shown to compensate their pH_{CF} when facing OA (Stumpp *et al.*, 2012a; Collard *et al.*, 2014; Moulin *et al.*, 2015) including close to CO_2 vents (Di Giglio et al., 2020b). This was linked to the high buffering capacity of their coelomic fluid, principally due to an accumulation of bicarbonate ions (Stumpp *et al.*, 2012b; Collard *et al.*, 2013b; 2014). *S. neumayeri* also has this high buffering capacity due to the high concentration in bicarbonate ions in its coelomic fluid (Collard *et al.*, 2014; present study). A pH-bicarbonate (Davenport) diagram compiling values available for the coelomic fluid (CF) of field specimens of *S. neumayeri* clearly indicates the absence of compensation for this species, despite the high bicarbonate concentration of the CF (Fig. 3). Such absence of compensation was reported in fasting sea urchins (Stumpp *et al.*, 2012b; Collard *et al.*, 2013b). *S. neumayeri* feeds on algae in shallow locations and benthic detritus in deeper locations (see Michel *et al.*, 2016, and references therein). In Deception Island, there were no macroalgae in the sampled stations and the sediment did not harbour much small macrofauna consumed by this species, like bryozoans. Therefore, sea urchins were probably detritus feeders, relying on an energetically rather poor diet. We hypothesize that the absence of pH_{CF} compensation in *S. neumayeri* in Deception Island was linked to poor food availability. The same explanation could be proposed for deep *S. neumayeri* from the Weddell Sea and Bransfield strait (Fig. 3) which were proven to be detritus feeders (Michel et al., 2016). This should be experimentally tested either in aquarium conditions or by caging experiments in Deception Island sites, with some sea urchins being offered macroalgae as food and others not.

So, in summary, the recorded acid-base physiologies of both species can be interpreted in the framework of known physiologies of temperate and tropical sea stars and sea urchins, but the moderate pH reduction in the acidified sites as well as possibly confounding factors like food shortage, prevent a definitive conclusion about the physiological answers to acidification of these two Antarctic species.

5.3. Mechanical properties of the skeleton of *Odontaster validus* and *Sterechinus neumayeri*

Mechanical properties of ambital plates of *S. neumayeri* were related neither to pH nor to metal contamination. In most temperate and tropical sea urchins, ambital plates were also shown to be resistant to OA (Holtmann *et al.*, 2013; Moulin *et al.*, 2015; Collard *et al.*, 2016; Di Giglio *et al.*, 2020b). Therefore, from this point of view, the response from *S. neumayeri* was similar to other sea urchins. In *O. validus*, ambulacral plates of specimens from BID had reduced mechanical properties compared to those of WHB (s_0, $Fmax_0$, E_0). However, neither s_0 nor E_0 appeared linked to pH_{SW} or metal concentrations. $Fmax_0$ was weakly linked ($R^2 > 0.14$) to metal contamination and pH_{SW} but no individual factor was significant and this effect is due to an impact of Cd on the plate I_2, indicating thinner or more porous plates. In the temperate *A. rubens*, Pb and Cd were shown to be linked to reduced F_{max} and Young's modulus (E) but this was not due to a reduced I_2 (Moureaux *et al.*, 2011). In the latter study, Pb contamination of the ambulacral plates was much higher (up to 37.6 µg $g^{-1}{}_{DW}$) but Cd contamination was much lower (up to 7.1 µg $g^{-1}{}_{DW}$). From the present study, it appears that Cd has only a minor effect on I_2, probably through an impact on plate growth (see Moureaux *et al.*, 2011, for a discussion).

Therefore, in the investigated sites of Deception Island, pH and metals do not have a major impact on the mechanical properties of the two investigated species, despite extremely high Cd concentrations (up to 171 $\mu g\ g^{-1}{}_{DW}$) in *O. validus*.

The skeleton of both species presented lower mechanical values than what was usually measured in the skeleton of temperate and tropical species. The Young's modulus of *O. validus* ambulacral plates is ten to twenty times lower than that of the temperate *A. rubens* from a metal contaminated station (Sørfjorden, Norway; Moureaux *et al.* 2011) (See Supplementary Table S16 for a review of literature). The Young's modulus, F_{max} and I_2 of the ambital plates of *S. neumayeri* are almost three orders of magnitude lower than those of the temperate *Paracentrotus lividus*, measured by Collard *et al.* (2016). This low skeletal resistance of Antarctic echinoderms could be linked to the low durophagous predation pressure established in Antarctic benthos from a long evolutionary time (reviewed in Peck, 2018). A second factor could be the subtidal habitat of all Antarctic echinoderms, away from wave exposure, due to ice scouring which prevents establishment and maintenance of populations in the intertidal zone and shallow subtidal. These factors would have favoured a low investment in skeleton formation at an evolutionary scale. The lower saturation state of Antarctic seawater is probably not linked to this low mechanical resistance in echinoderms as the process of calcification is not depending on carbonate ions but on bicarbonate ions (see Dubois, 2014; Collard *et al.*, 2015, for a discussion). Besides, the major limiting factor for calcifiers is the efficient elimination of protons (Bach, 2015; Suwa et al., 2014).

For both species, food availability in the different stations might be a possible explanation for the differences observed in the skeletal properties between stations (Ebert, 2013). Food availability in the caldera is generally low (Cranmer et al., 2003) but densities of both species are high and intraspecific competition for food might be severe, especially in BID station where the highest abundances of both species were recorded (24 individuals m^{-2} for *O. validus* and

182-285 individuals m^{-2} for *S. neumayeri*) (Angulo-Preckler *et al.*, 2017a). Low food availability and high competition could result in a lower energy allocation to skeleton formation.

5.4. Metals contamination of *Odontaster validus* and *Sterechinus neumayeri*

The ratios between metal concentrations in the compartments and the sediment ranged between 0.02 and 12. Values of Fe, Pb, Zn and Cu concentrations in the different compartments of both species were similar to values previously reported in the same species by other authors (de Moreno *et al.*, 1997; Riva *et al.*, 2004; Grotti *et al.*, 2008; Webb *et al.*, 2020). Remarkably high concentrations of cadmium for the sea star *O. validus* were recorded with 2000 times more Cd in the integument of this species than in the sediment. Such high Cd concentrations in *O. validus* were also reported by previous studies (see Webb *et al.*, 2020, and references therein). This was attributed to the transport of the upper circumpolar deep water onto the Western Antarctic Peninsula shelf, resulting in high algal backgrounds that are transferred along the food web (Webb et al., 2020). The long life span of *O. validus* (McClintock *et al.*, 1988) further facilitates bioaccumulation of Cd, which is in part trapped in the skeleton (Temara *et al.*, 1997; Moureaux *et al.*, 2011). Cd concentrations measured in *S. neumayeri* were similar to those measured by Grotti *et al.* (2008) in Terra Nova Bay (Ross Sea). They were much lower than those measured in another primary consumer in the WAP, the grazer *Nacella concinna* (Webb et al., 2020). This probably points out to substantial differences in food sources between the considered sites, the Deception Island benthos being poor in macroalgae.

Most metal concentrations in the integument were negatively correlated to pH_{CF} (except Cd in *O. validus*) which could indicate a higher bioavailability with decreasing pH_{SW}. However, most correlation coefficients were rather low, indicating that pH was not the main factor affecting metal bioconcentration in these species. On the contrary, no metal concentration was correlated to pH in the digestive compartments of both species. This could be linked to the naturally low pH environment of these organs, making the changes in pH_{CF} unimportant.

6. Conclusion

Although the vents of Deception Island caldera offer interesting opportunities to test hypotheses dealing with OA and metal contamination in benthic organisms, the relatively moderate pH_{SW} decrease in the studied sites as well as possibly confounding factors, principally linked to food supply and quality, are important limitations. These could be overcome by translocating organisms along the pH gradient and caging them with or without added food. These translocations should be accompanied by the deployment of a continuous pH/temperature recorder to document possible variability of the sea water pH and/or temperature during the experiment. Facilities available in the Base Antarctica Gabriel de Castilla, as well as the sheltered character of the caldera, make such experiments feasible in the future.

7. Acknowledgements

SD. was a holder of a FRIA grant. PD. is a Research Director of the National Fund for Scientific Research (FRS-FNRS; Belgium). This project has been feasible thanks to a collaboration with the University of Barcelona through the BLUEBIO Project (CTM2016-78901/ANT) to CA, the Spanish Station: Base Antártica Gabriel de Castilla and the Spanish Polar Committee. We would like to thank Prof. I. Eeckhaut, P. Flammang, and Mr. N. Puozzo for providing access to the SEM. The access to the IRMS for DIC measurements was provided by Prof. F. Dehairs and Dr. D. Verstraeten. We thank Blanca Figuerola for the measurements of seawater parameters at several stations of Deception Island. We thank two anonymous reviewers for their constructive comments. The study was supported by FNRS grant n° J.0219.16 SOFTECHI. This is contribution no. 012 to the rECTO project (contract no. BR/154/A1/RECTO). This is an AntECO (SCAR) contribution.

8. Bibliography

Agüera, A., Collard, M., Jossart, Q., Moreau, C., Danis, B., 2015. Parameter Estimations of Dynamic Energy Budget (DEB) Model over the Life History of a Key Antarctic Species: The Antarctic Sea Star Odontaster validus Koehler, 1906. PLoS One 10, e0140078. https://doi.org/10.1371/journal.pone.0140078

Andersson, A.J., MacKenzie, F.T., Lerman, A., 2005. Coastal ocean and carbonate systems in the high CO2 world of the anthropocene. Am. J. Sci. 305, 875–918. https://doi.org/10.2475/ajs.305.9.875

Angulo-Preckler, C., Figuerola, B., Núñez-Pons, L., Moles, J., Martín-Martín, R., Rull-Lluch, J., Gómez-Garreta, A., Avila, C., 2018. Macrobenthic patterns at the shallow marine waters in the caldera of the active volcano of Deception Island, Antarctica. Cont. Shelf Res. 157, 20–31. https://doi.org/10.1016/j.csr.2018.02.005

Angulo-Preckler, C., Leiva, C., Avila, C., Taboada, S., 2017a. Macroinvertebrate communities from the shallow soft-bottoms of Deception Island (Southern Ocean): A paradise for opportunists. Mar. Environ. Res. 127, 62–74. https://doi.org/10.1016/j.marenvres.2017.03.008

Angulo-Preckler, C., Tuya, F., Avila, C., 2017b. Abundance and size patterns of echinoderms in coastal soft-bottoms at Deception Island (South Shetland Islands, Antarctica). Cont. Shelf Res. 137, 131–141. https://doi.org/10.1016/j.csr.2016.12.010

Appelhans, Y., Thomsen, J., Pansch, C., Melzner, F., Wahl, M., 2012. Sour times: seawater acidification effects on growth, feeding behaviour and acid–base status of Asterias rubens and Carcinus maenas. Mar. Ecol. Prog. Ser. 459, 85–98. https://doi.org/10.3354/meps09697

Appelhans, Y.S., Thomsen, J., Opitz, S., Pansch, C., Melzner, F., Wahl, M., 2014. Juvenile sea stars exposed to acidification decrease feeding and growth with no acclimation potential. Mar. Ecol. Prog. Ser. 509, 227–239. https://doi.org/10.3354/meps10884

Arntz, W.E., Gallardo, V.A., 1994. Antarctic Benthos: Present Position and Future Prospects. Antarct. Sci. 243–277. https://doi.org/10.1007/978-3-642-78711-9_16

Bach, L.T., 2015. Reconsidering the role of carbonate ion concentration in calcification by marine organisms. Biogeosciences 12, 4939–4951. https://doi.org/10.5194/bg-12-4939-2015

Barnes, D.K.A., Linse, K., Enderlein, P., Smale, D., Fraser, K.P.P., Brown, M., 2008. Marine richness and gradients at Deception Island, Antarctica. Antarct. Sci. 20, 271–279. https://doi.org/10.1017/S0954102008001090

Berrocoso, M., Prates, G., Fernández-Ros, A., Peci, L.M., de Gil, A., Rosado, B., Páez, R., Jigena, B., 2018. Caldera unrest detected with seawater temperature anomalies at Deception Island, Antarctic Peninsula. Bull. Volcanol. 80. https://doi.org/10.1007/s00445-018-1216-2

Bray, L., Pancucci-Papadopoulou, M.A., Hall-spencer, J.M., 2014. Sea urchin response to rising pCO2 shows ocean acidification may fundamentally alter the chemistry of marine skeletons. Mediterr. Mar. Sci. https://doi.org/10.12681/mms.579

Burns, W., 2008. Anthropogenic carbon dioxide emissions and ocean acidification: the potential impacts on ocean biodiversity. Sav. Biol. Divers. 187–202.

Bütikofer, L., Stawarczyk, B., Roos, M., 2015. Two regression methods for estimation of a two-parameter Weibull distribution for reliability of dental materials. Dent. Mater. 31, e33–e50. https://doi.org/10.1016/j.dental.2014.11.014

Byrne, M., Ho, M. a., Koleits, L., Price, C., King, C.K., Virtue, P., Tilbrook, B., Lamare, M., 2013. Vulnerability of the calcifying larval stage of the Antarctic sea urchin Sterechinus neumayeri to near-future ocean acidification and warming. Glob. Chang. Biol. 19, 2264–2275. https://doi.org/10.1111/gcb.12190

Caldeira, K., Wickett, M.E., 2003. Anthropogenic carbon and ocean pH. Nature 425, 365. https://doi.org/10.1038/425365a

Collard, M., Catarino, A.I., Bonnet, S., Flammang, P., Dubois, P., 2013a. Effects of CO2-induced ocean acidification on physiological and mechanical properties of the starfish Asterias rubens. J. Exp. Mar. Bio. Ecol. 446, 355–362. https://doi.org/10.1016/j.jembe.2013.06.003

Collard, M., De Ridder, C., David, B., Dehairs, F., Dubois, P., 2015. Could the acid-base status of Antarctic sea urchins indicate a better-than-expected resilience to near-future ocean acidification? Glob. Chang. Biol. 21, 605–17. https://doi.org/10.1111/gcb.12735

Collard, M., Dery, A., Dehairs, F., Dubois, P., 2014. Comparative Biochemistry and Physiology , Part A Euechinoidea and Cidaroidea respond differently to ocean acidi fi cation. Comp. Biochem. Physiol. Part A 174, 45–55. https://doi.org/10.1016/j.cbpa.2014.04.011

Collard, M., Laitat, K., Moulin, L., Catarino, A.I., Grosjean, P., Dubois, P., 2013b. Buffer capacity of the coelomic fluid in echinoderms. Comp. Biochem. Physiol. - A Mol. Integr. Physiol. 166, 19–206. https://doi.org/10.1016/j.cbpa.2013.06.002

Collard, M., Rastrick, S.P.S., Calosi, P., Demolder, Y., Dille, J., Findlay, H.S., Hall-spencer, J.M., Milazzo, M., Moulin, L., Widdicombe, S., Dehairs, F., Dubois, P., 2016. The impact of ocean acidification and warming on the skeletal mechanical properties of the sea urchin Paracentrotus lividus from laboratory and field observations. ICES J. 12. https://doi.org/10.1093/icesjms/fsv018

Coteur, G., Danis, B., Wantier, P., Pernet, P., Dubois, P., 2005. Increased phagocytic activity in contaminated seastars (Asterias rubens) collected in the Southern Bight of the North Sea. Mar. Pollut. Bull. 50, 1295–1302. https://doi.org/10.1016/j.marpolbul.2005.04.038

Coteur, G., Gosselin, P., Wantier, P., Chambost-Manciet, Y., Danis, B., Pernet, P., Warnau, M., Dubois, P., 2003. Echinoderms as bioindicators, bioassays, and impact assessment tools of sediment-associated metals and PCBs in the North Sea. Arch. Environ. Contam. Toxicol. 45, 190–202. https://doi.org/10.1007/s00244-003-0199-x

Cranmer, T.L., Ruhl, H.A., Baldwin, R.J., Kaufmann, R.S., 2003. Spatial and temporal variation in the abundance, distribution and population structure of epibenthic megafauna in Port Foster, Deception Island. Deep. Res. Part II Top. Stud. Oceanogr. 50, 1821–1842. https://doi.org/10.1016/S0967-0645(03)00093-6

de Moreno, J.E.A., Gerpe, M.S., Moreno, V.J., Vodopivez, C., 1997. Heavy metals in Antarctic organisms. Polar Biol. 17, 131–140.

Deheyn, D.D., Gendreau, P., Baldwin, R.J., Latz, M.I., 2005. Evidence for enhanced bioavailability of trace elements in the marine ecosystem of Deception Island, a volcano in Antarctica. Mar. Environ. Res. 60, 1–33. https://doi.org/10.1016/j.marenvres.2004.08.001

Dell'Acqua, O., Ferrando, S., Chiantore, M., Asnaghi, V., 2019. The impact of ocean acidification on the gonads of three key Antarctic benthic macroinvertebrates. Aquat. Toxicol. 210, 19–29. https://doi.org/10.1016/j.aquatox.2019.02.012

DelValls, T.A., Dickson, A.G., 1998. The pH of buffers based on 2-amino-2-hydroxymethyl-1,3-propanediol ('tris') in synthetic sea water. Deep. Res. Part I Oceanogr. Res. Pap. 45, 1541–1554. https://doi.org/10.1016/S0967-0637(98)00019-3

Di Giglio, S., Lein, E., Hu, M.Y., Stumpp, M., Melzner, F., Malet, L., Pernet, P., Dubois, P., 2020a. Skeletal integrity of a marine keystone predator (Asterias rubens) threatened by ocean acidification. J. Exp. Mar. Bio. Ecol. 526, 151335. https://doi.org/10.1016/j.jembe.2020.151335

Di Giglio, S., Spatafora, D., Milazzo, M., M'Zoudi, S., Zito, F., Dubois, P., Costa, C., 2020b. Are control of extracellular acid-base balance and regulation of skeleton genes linked to resistance to ocean acidification in adult sea urchins? Sci. Total Environ. 720, 137443. https://doi.org/10.1016/j.scitotenv.2020.137443

Dickson, A.G., 1990. Standard potential of the reaction: AgCl(s) + 1 2H2(g) = Ag(s) + HCl(aq), and and the standard acidity constant of the ion HSO4- in synthetic sea water from 273.15 to 318.15 K. J. Chem. Thermodyn. 22, 113–127. https://doi.org/10.1016/0021-9614(90)90074-Z

Dickson, A.G., Millero, F.J., 1987. A comparison of the equilibrium constants for the dissociation of carbonic acid in seawater media. Deep Sea Res. Part A, Oceanogr. Res. Pap. 34, 1733–1743. https://doi.org/10.1016/0198-0149(87)90021-5

Doncaster, C.P., Davey, A.J.H., 2007. Analysis of variance and covariance: how to choose and construct models for the life sciences. https://doi.org/10.1080/02664760902885203

Dubois, P., 2014. The skeleton of postmetamorphic echinoderms in a changing world. Biol. Bull. 226, 223–236.

Duquette, A., Vohra, Y.K., McClintock, J.B., Angus, R.A., 2018. Near-future temperature reduces Mg/Ca ratios in the major skeletal components of the common subtropical sea urchin Lytechinus variegatus. J. Exp. Mar. Bio. Ecol. 509, 1–7. https://doi.org/10.1016/j.jembe.2018.08.007

Ebert, T.A., 2013. Growth and survival of postsettlement sea urchins, Developments in Aquaculture and Fisheries Science. Elsevier. https://doi.org/10.1016/B978-0-12-396491-5.00007-1

Ericson, J.A., Ho, M.A., Miskelly, A., King, C.K., Virtue, P., Tilbrook, B., Byrne, M., 2012. Combined effects of two ocean change stressors, warming and acidification, on fertilization and early development of the Antarctic echinoid Sterechinus neumayeri. Polar Biol. 35, 1027–1034. https://doi.org/10.1007/s00300-011-1150-7

Ericson, J.A., Lamare, M.D., Morley, S.A., Barker, M.F., 2010. The response of two ecologically important Antarctic invertebrates (Sterechinus neumayeri and Parborlasia corrugatus) to reduced seawater pH: Effects on fertilisation and embryonic development. Mar. Biol. 157, 2689–2702. https://doi.org/10.1007/s00227-010-1529-y

Fabricius, K.E., Langdon, C., Uthicke, S., Humphrey, C., Noonan, S., De'ath, G., Okazaki, R., Muehllehner, N., Glas, M.S., Lough, J.M., 2011. Losers and winners in coral reefs acclimatized to elevated carbon dioxide concentrations. Nat. Clim. Chang. 1, 165–169. https://doi.org/10.1038/nclimate1122

Feely, R. a, Sabine, C.L., Lee, K., Berelson, W., Kleypas, J., Fabry, V.J., Millero, F.J., Anonymous, 2004. Impact of anthropogenic CO (sub 2) on the CaCO (sub 3) system in the oceans. Science (80-.). 305, 362–366.

Flexas, M.M., Arias, M.R., Ojeda, M.A., 2017. Hydrography and dynamics of Port Foster, Deception Island, Antarctica. Antarct. Sci. 29, 83–93. https://doi.org/10.1017/S0954102016000444

Foo, S.A., Sparks, K.M., Uthicke, S., Karelitz, S., Barker, M., Byrne, M., Lamare, M., 2016. Contributions of genetic and environmental variance in early development of the Antarctic sea urchin Sterechinus neumayeri in response to increased ocean temperature and acidification. Mar. Biol. 163. https://doi.org/10.1007/s00227-016-2903-1

Gillikin, D.P., Lorrain, A., Meng, L., Dehairs, F., 2010. A large metabolic carbon contribution to the δ 13C record in marine aragonitic bivalve shells.

Gonzalez-Bernat, M.J., Lamare, M., Barker, M., 2012. Effects of reduced seawater pH on fertilisation, embryogenesis and larval development in the Antarctic seastar Odontaster validus. Polar Biol. https://doi.org/10.1007/s00300-012-1255-7

Grotti, M., Soggia, F., Lagomarsino, C., Riva, S.D., Goessler, W., Francesconi, K.A., 2008. Natural variability and distribution of trace elements in marine organisms from Antarctic coastal environments. Antarct. Sci. 20, 39–51. https://doi.org/10.1017/S0954102007000831

Guerra, R., Fetter, E., Ceschim, L.M.M., Martins, C.C., 2011. Trace metals in sediment cores from Deception and Penguin Islands (South Shetland Islands, Antarctica). Mar. Pollut. Bull. 62, 2571–2575. https://doi.org/10.1016/j.marpolbul.2011.08.012

Gutt, J., Starmans, A., Dieckmann, G., 1998. Phytodetritus deposited on the Antarctic shelf and upper slope: Its relevance for the benthic system. J. Mar. Syst. 17, 435–444. https://doi.org/10.1016/S0924-7963(98)00054-2

Hall-Spencer, J.M., Rodolfo-Metalpa, R., Martin, S., Ransome, E., Fine, M., Turner, S.M., Rowley, S.J., Tedesco, D., Buia, M.-C., 2008. Volcanic carbon dioxide vents show ecosystem effects of ocean acidification. Nature 454, 96–99. https://doi.org/10.1038/nature07051

Hernroth, B., Baden, S., Thorndyke, M., Dupont, S., 2011. Immune suppression of the echinoderm Asterias rubens (L.) following long-term ocean acidification. Aquat. Toxicol. 103, 222–4. https://doi.org/10.1016/j.aquatox.2011.03.001

Holtmann, W.C., Stumpp, M., Gutowska, M.A., Syr??, S., Himmerkus, N., Melzner, F., Bleich, M., 2013. Maintenance of coelomic fluid pH in sea urchins exposed to elevated CO2: The role of body cavity epithelia and stereom dissolution. Mar. Biol. 160, 2631–2645. https://doi.org/10.1007/s00227-013-2257-x

Ingels, J., Vanreusel, A., Brandt, A., Catarino, A.I., David, B., De Ridder, C., Dubois, P., Gooday, A.J., Martin, P., Pasotti, F., Robert, H., 2012. Possible effects of global environmental changes on Antarctic benthos: a synthesis across five major taxa. Ecol. Evol. 2, 453–85. https://doi.org/10.1002/ece3.96

IPCC, 2014. Intergovernmental Panel on Climate Change. Climate Change 2014 Synthesis Report.

Jerez, S., Motas, M., Palacios, M.J., Valera, F., Cuervo, J.J., Barbosa, A., 2011. Concentration of trace elements in feathers of three Antarctic penguins: geographical and interspecific differences. Environ. Pollut. 159, 2412–9. https://doi.org/10.1016/j.envpol.2011.06.036

Jewett, L., Romanou, A., 2017. Ocean Acidification and Other Ocean Changes. Clim. Sci. Spec. Rep. Fourth Natl. Clim. Assessment, Vol. I I, 364–392. https://doi.org/10.7930/J0QV3JQB

Kapsenberg, L., Hofmann, G.E., 2014. Signals of resilience to ocean change: High thermal tolerance of early stage Antarctic sea urchins (Sterechinus neumayeri) reared under present-day and future pCO2and temperature. Polar Biol. 37. https://doi.org/10.1007/s00300-014-1494-x

Kroeker, K.J., Micheli, F., Gambi, M.C., 2012. Ocean acidification causes ecosystem shifts via altered competitive interactions. Nat. Clim. Chang. 3, 156–159. https://doi.org/10.1038/nclimate1680

Kusakabe, M., Nagao, K., Ohba, T., Seo, J.H., Park, S.H., Lee, J.I., Park, B.K., 2009. Noble gas and stable isotope geochemistry of thermal fluids from deception Island, Antarctica. Antarct. Sci. 21, 255–267. https://doi.org/10.1017/S0954102009001783

Linares, C., Vidal, M., Canals, M., Kersting, D.K., Amblas, D., Aspillaga, E., Cebrián, E., Delgado-Huertas, A., Díaz, D., Garrabou, J., Hereu, B., Navarro, L., Teixidó, N., Ballesteros, E., 2015. Persistent natural acidification drives major distribution shifts in marine benthic ecosystems. Proc. R. Soc. B Biol. Sci. 282, 20150587. https://doi.org/10.1098/rspb.2015.0587

Lovell, L.L., Trego, K.D., 2003. The epibenthic megafaunal and benthic infaunal invertebrates of Port Foster, Deception Island (South Shetland Islands, Antarctica). Deep. Res. Part II Top. Stud. Oceanogr. 50, 1799–1819. https://doi.org/10.1016/S0967-0645(03)00087-0

Marsh, G., 2008. Seawater pH and Anthropogenic Carbon Dioxide. arXiv Prepr.

arXiv0810.3596 1–15.

Massom, R.A., Stammerjohn, S.E., 2010. Antarctic sea ice change and variability e Physical and ecological implications. Polar Sci. 4, 149–186. https://doi.org/10.1016/j.polar.2010.05.001

McClintock, J.B., Amsler, M.O., Angus, R.A., Challener, R.C., Schram, J.B.S., Amsler, C.D., Mah, C.L., Cuce, J., Baker, B.J., 2011. The Mg-Calcite composition of Antarctic echinoderms: important implications for predicting the impacts of ocean acidification. J. Geol. 119, 457–466.

McNeil, B.I., Matear, R.J., 2008. Southern Ocean acidification: A tipping point at 450-ppm atmospheric CO2. Proc. Natl. Acad. Sci. U. S. A. 105, 18860–18864. https://doi.org/10.1073/pnas.0806318105

Mehrbach, C., Culberson, C.H., Hawley, J.E., Pytkowicz, R.M., 1973. Measurement of the apparent dissociation constants of carbonic acid in seawater at atmospheric pressure. Limnol. Oceanogr. 18, 897–907. https://doi.org/10.4319/lo.1973.18.6.0897

Michel, L.N., David, B., Dubois, P., Lepoint, G., De Ridder, C., 2016. Trophic plasticity of Antarctic echinoids under contrasted environmental conditions. Polar Biol. 39, 913–923. https://doi.org/10.1007/s00300-015-1873-y

Millero, F.J., Woosley, R., Ditrolio, B., Waters, J., 2009. Effect of ocean acidification on the speciation of metals in seawater. Oceanography. https://doi.org/10.5670/oceanog.2009.98

Monteiro, T., Kerr, R., Orselli, I.B.M., Lencina-Avila, J.M., 2020. Towards an intensified summer CO2 sink behaviour in the Southern Ocean coastal regions. Prog. Oceanogr.

102267. https://doi.org/10.1016/J.POCEAN.2020.102267

Montes-Hugo, M., Doney, S.C., Ducklow, H.W., Fraser, W., Martinson, D., Stammerjohn, S.E., Schofield, O., 2009. Recent Changes in Phytoplankton Communities Associated with Rapid Regional Climate Change Along the Western Antarctic Peninsula. Science (80-.). 323, 1470–1473. https://doi.org/10.1126/science.1164533

Morley, S.A., Suckling, C.C., Clark, M.S., Cross, E.L., Peck, L.S., 2016. Long-term effects of altered pH and temperature on the feeding energetics of the Antarctic sea urchin, Sterechinus neumayeri. Biodiversity 17, 34–45. https://doi.org/10.1080/14888386.2016.1174956

Morse, J.W., Andersson, A.J., Mackenzie, F.T., Blake, D.F., Peacor, D.R., Allard, L.F., Berman, A., Addadi, L., Weiner, S., Tsafnat, N., Fitz Gerald, J.D., Le, H.N., Stachurski, Z.H., Iglikowska, A., Najorka, J., Voronkov, A., Chełchowski, M., Kukliński, P., Ihli, J., Wong, W.C., Noel, E.H., Kim, Y.-Y., Kulak, A.N., Christenson, H.K., Duer, M.J., Meldrum, F.C., Meng, Y., Guo, Z., Yao, H., Yeung, K.W.K., Thiyagarajan, V., Märkel, K., Kubanek, F., Willgallis, A., Ma, Y., Cohen, S.R., Addadi, L., Weiner, S., Politi, Y., Arad, T., Klein, E., Weiner, S., Addadi, L., McLaughlin, K., Nezlin, N.P., Weisberg, S.B., Dickson, A.G., Ashley, J., Booth, T., Cash, C.L., Feit, A., Gully, J.R., Howard, M., Johnson, S., Latker, A., Mengel, M.J., Robertson, G.L., Steele, A., Terriquez, L., Albeck, S., Addadi, L., Weiner, S., Füger, A., Konrad, F., Leis, A., Dietzel, M., Mavromatis, V., Cheng, X., Varona, P.L., Olszta, M.J., Gower, L.B., Chen, P.Y., Lin, A.Y.M., Lin, Y.S., Seki, Y., Stokes, A.G., Peyras, J., Olevsky, E.A., Meyers, M.A., McKittrick, J., Naviaux, J.D., Subhas, A. V., Dong, S., Rollins, N.E., Liu, X., Byrne, R.H., Berelson, W.M., Adkins, J.F., Dong, S., Berelson, W.M., Adkins, J.F., Emlet, R.B., 2019. Ultrastructural and microanalytical results from echinoderm calcite: Implications for biomineralization and diagenesis of skeletal material. Geochim. Cosmochim. Acta 307, 85–90. https://doi.org/10.1016/j.jcrysgro.2007.07.006

Moulin, L., Grosjean, P., Leblud, J., Batigny, A., Collard, M., Dubois, P., 2015. Long-term mesocosms study of the effects of ocean acidification on growth and physiology of the sea urchin Echinometra mathaei. Mar. Environ. Res. 103, 103–114. https://doi.org/10.1016/j.marenvres.2014.11.009

Moulin, L., Grosjean, P., Leblud, J., Batigny, A., Dubois, P., 2014. Impact of elevated pCO2 on acid-base regulation of the sea urchin Echinometra mathaei and its relation to resistance to ocean acidification: A study in mesocosms. J. Exp. Mar. Bio. Ecol. 457, 97–104. https://doi.org/10.1016/j.jembe.2014.04.007

Moureaux, C., Simon, J., Mannaerts, G., Catarino, A.I., Pernet, P., Dubois, P., 2011. Effects of field contamination by metals (Cd, Cu, Pb, Zn) on biometry and mechanics of echinoderm ossicles. Aquat. Toxicol. 105, 698–707. https://doi.org/10.1016/j.aquatox.2011.09.007

Orr, J.C., Fabry, V.J., Aumont, O., Bopp, L., Doney, S.C., Feely, R.M., Gnanadesikan, A., Gruber, N., Ishida, A., Key, R.M., Lindsay, K., Maier-reimer, E., Matear, R., Monfray, P., Mouchet, a., Najjar, R.G., Plattner, G.K., Rodgers, K.B., Sabine, C.L., Sarmiento, J.L., Schlitzer, R., Slater, R.D., Totterdell, I.J., Weirig, M.F., Yamanaka, Y., Yool, a., Matear, Richard, 2005. Anthropogenic Decline in High-Latitude Ocean Carbonate by 2100. Nature 437, 681–686.

Peck, L., Webb, K., Miller, a, Clark, M., Hill, T., 2008. Temperature limits to activity, feeding and metabolism in the Antarctic starfish Odontaster validus. Mar. Ecol. Prog. Ser. 358, 181–189. https://doi.org/10.3354/meps07336

Peck, L.S., 2018. Antarctic Marine Biodiversity: Adaptations, Environments and Responses to Change. Oceanogr. Mar. Biol. 105–236. https://doi.org/10.1201/9780429454455-3

Peck, L.S., 2005. Prospects for surviving climate change in Antarctic aquatic species. Front. Zool. https://doi.org/10.1186/1742-9994-2-9

Pierrot, D., Lewis, E., Wallace, D.W.R., 2006. MS Excel program developed for CO2 system calculations, in: ORNL/CDIAC-105a. Carbon Dioxide Information Analysis Center, Oak Ridge National Laboratory, US Department of Energy, Oak Ridge, Tennessee.

Rey, J., Somoza, L., Martínez-Frías, J., 1995. Tectonic, volcanic, and hydrothermal event sequence on Deception Island (Antarctica). Geo-Marine Lett. 15, 1–8. https://doi.org/10.1007/BF01204491

Riva, S.D., Abelmoschi, M.L., Magi, E., Soggia, F., 2004. The utilization of the Antarctic environmental specimen bank (BCAA) in monitoring Cd and Hg in an Antarctic coastal area in Terra Nova Bay (Ross Sea - Northern Victoria Land). Chemosphere 56, 59–69. https://doi.org/10.1016/j.chemosphere.2003.12.026

Rogers, A.D., Frinault, B.A.V., Barnes, D.K.A., Bindoff, N.L., Downie, R., Ducklow, H.W., Friedlaender, A.S., Hart, T., Hill, S.L., Hofmann, E.E., Linse, K., McMahon, C.R., Murphy, E.J., Pakhomov, E.A., Reygondeau, G., Staniland, I.J., Wolf-Gladrow, D.A., Wright, R., 2019. Antarctic Futures: An Assessment of Climate-Driven Changes in Ecosystem Structure, Function, and Service Provisioning in the Southern Ocean. Ann. Rev. Mar. Sci. 12, 1–34. https://doi.org/10.1146/annurev-marine-010419-011028

Sabine, C.L., Feely, R.A., Gruber, N., Key, R.M., Lee, K., Bullister, J.L., Wanninkhof, R., Wong, C.S., Wallace, D.W.R., Tilbrook, B., Millero, F.J., Peng, T.H., Kozyr, A., Ono, T., Rios, A.F., 2004. The oceanic sink for anthropogenic CO2. Science (80-.). 305, 367–

371. https://doi.org/10.1126/science.1097403

Schneider, C.A., Rasband, W.S., Eliceiri, K., 2012. NIH Image to ImageJ: 25 years of image analysis. Nat. Methods 9(7), 671–675.

Sewell, M.A., Hofmann, G.E., 2011. Antarctic echinoids and climate change: A major impact on the brooding forms. Glob. Chang. Biol. 17, 734–744. https://doi.org/10.1111/j.1365-2486.2010.02288.x

Shilling, F.M., Manahan, D.T., 1994. Energy metabolism and amino acid transport during early development of Antarctic and temperate echinoderms. Biol. Bull. 187, 398–407. https://doi.org/10.2307/1542296

Solomon, S., Plattmner, G.-K., Knutti, R., Friedlingstein, P., 2008. Irreversible climate change due to carbon dioxide emissions. PNAS 56, 581–592. https://doi.org/10.1073/pnas.0812721106

Somoza, L., Martínez-Frías, J., Smellie, J.L., Rey, J., Maestro, A., 2004. Evidence for hydrothermal venting and sediment volcanism discharged after recent short-lived volcanic eruptions at Deception Island, Bransfield Strait, Antarctica. Mar. Geol. 203, 119–140. https://doi.org/10.1016/S0025-3227(03)00285-8

Steinacher, M., Joos, F., 2016. Transient Earth system responses to cumulative carbon dioxide emissions : linearities , uncertainties , and probabilities in an observation-constrained model ensemble 1071–1103. https://doi.org/10.5194/bg-13-1071-2016

Stumpp, Meike, Hu, M.Y., Melzner, F., Gutowska, M.A., Dorey, N., Himmerkus, N., Holtmann, W.C., Dupont, S.T., Thorndyke, M.C., Bleich, M., 2012a. Acidified seawater impacts sea urchin larvae pH regulatory systems relevant for calcification. Proc. Natl.

Acad. Sci. https://doi.org/10.1073/pnas.1209174109

Stumpp, M, Trübenbach, K., Brennecke, D., Hu, M.Y., Melzner, F., 2012b. Resource allocation and extracellular acid – base status in the sea urchin Strongylocentrotus droebachiensis in response to CO 2 induced seawater acidification 111, 194–207. https://doi.org/10.1016/j.aquatox.2011.12.020

Sturz, A.A., Gray, S.C., Dykes, K., King, A., Radtke, J., 2003. Seasonal changes of dissolved nutrients within and around Port Foster Deception Island, Antarctica. Deep. Res. Part II Top. Stud. Oceanogr. 50, 1685–1705. https://doi.org/10.1016/S0967-0645(03)00086-9

Suckling, C.C., Clark, M.S., Richard, J., Morley, S.A., Thorne, M.A.S., Harper, E.M., Peck, L.S., 2015. Adult acclimation to combined temperature and pH stressors significantly enhances reproductive outcomes compared to short-term exposures. J. Anim. Ecol. 84, 773–784. https://doi.org/10.1111/1365-2656.12316

Suszczewski, R.S.R., Janecki, T., Domanov, M.M., 2010. Starvation and Chemoreception in Antarctic Benthic Invertebrates 37, 56–62. https://doi.org/10.1134/S1062359010010085

Sutherland, R.A., 2002. Comparison between non-residual Al, Co, Cu, Fe, Mn, Ni, Pb and Zn released by a three-step sequential extraction procedure and a dilute hydrochloric acid leach for soil and road deposited sediment. Appl. Geochemistry 17, 353–365. https://doi.org/10.1016/S0883-2927(01)00095-6

Suwa, R., Hatta, M., Ichikawa, K., 2014. Proton-transfer reaction dynamics and energetics in calcification and decalcification. Chem. - A Eur. J. 1–7. https://doi.org/10.1002/chem.201402210

Temara, A., Warnau, M., Jangoux, M., Dubois, P., 1997. Factors influencing the concentrations of heavy metals in the asteroid Asterias rubens L. (Echinodermata). Sci. Total Environ. 203, 51–63. https://doi.org/10.1016/S0048-9697(97)00134-4

Turley, C., 2008. Impacts of changing ocean chemistry in a high-CO2 world. Mineral. Mag. 72, 359–362. https://doi.org/10.1180/minmag.2008.072.1.359

Turner, J., Barrand, N.E., Bracegirdle, T.J., Convey, P., Hodgson, D.A., Jarvis, M., Jenkins, A., Marshall, G., Meredith, M.P., Roscoe, H., Shanklin, J., French, J., Goosse, H., Guglielmin, M., Gutt, J., Jacobs, S., Kennicutt, M.C., Masson-Delmotte, V., Mayewski, P., Navarro, F., Robinson, S., Scambos, T., Sparrow, M., Summerhayes, C., Speer, K., Klepikov, A., 2014. Antarctic climate change and the environment: An update. Polar Rec. (Gr. Brit). 50, 237–259. https://doi.org/10.1017/S0032247413000296

Tyrrell, T., 2011. Anthropogenic modification of the oceans. Philos. Trans. A. Math. Phys. Eng. Sci. 369, 887–908. https://doi.org/10.1098/rsta.2010.0334

Vlček, V., Juřička, D., Míková, J., 2017. Heavy metal concentration in selected soils and sediments of Livingston Island, Deception Island, King George Island, James Ross Island (Antarctica). Czech Polar Reports 7, 18–33. https://doi.org/10.5817/CPR2017-1-3

Watson, S.-A., Peck, L.S., Tyler, P. a., Southgate, P.C., Tan, K.S., Day, R.W., Morley, S. a., 2012. Marine invertebrate skeleton size varies with latitude, temperature and carbonate saturation: implications for global change and ocean acidification. Glob. Chang. Biol. 18, 3026–3038. https://doi.org/10.1111/j.1365-2486.2012.02755.x

Watson, S.A., Morley, S.A., Bates, A.E., Clark, M.S., Day, R.W., Lamare, M., Martin, S.M., Southgate, P.C., Tan, K.S., Tyler, P.A., Peck, L.S., 2014. Low global sensitivity of metabolic rate to temperature in calcified marine invertebrates. Oecologia 174, 45–54. https://doi.org/10.1007/s00442-013-2767-8

Webb, A.E., Pomponi, S.A., van Duyl, F.C., Reichart, G.J., de Nooijer, L.J., 2019. pH Regulation and Tissue Coordination Pathways Promote Calcium Carbonate Bioerosion by Excavating Sponges. Sci. Rep. 9, 1–10. https://doi.org/10.1038/s41598-018-36702-8

Webb, A.L., Hughes, K.A., Grand, M.M., Lohan, M.C., Peck, L.S., 2020. Sources of elevated heavy metal concentrations in sediments and benthic marine invertebrates of the western Antarctic Peninsula. Sci. Total Environ. 698, 134268. https://doi.org/10.1016/j.scitotenv.2019.134268

Effects of ocean acidification on acid-base physiology, skeleton properties, and metal contamination in two echinoderms from vent sites in Deception Island, Antarctica

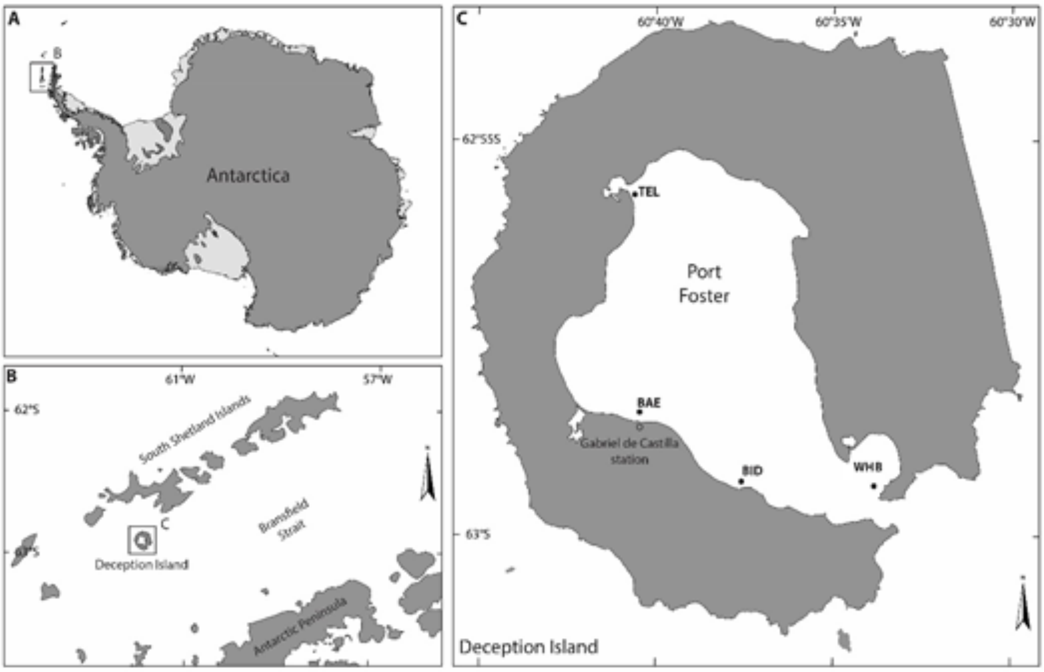

Figure 1. Sampling area **(A)** Global map of Antarctica; **(B)** South Shetland Islands; **(C)** Deception Island (sampling stations marked with a dot) **WHB**: Whaler´s Bay; **BID**: Bidones Point; **BAE**: Antarctic Spanish Base Gabriel de Castilla: Spanish Antarctic Station; **TEL**: Telephone Bay.

Table 1. Seawater physico-chemical parameters at the four stations of Deception Island on the day of sampling (Mean ± SD, n=3). TA, pCO_2, HCO_3^-, CO_3^{2-}, $\Omega_{calcite}$ and $\Omega_{aragonite}$ were calculated with CO2SYS software with pH_T and DIC values. Means sharing the same superscript are not significantly different ($\alpha = 0.05$).

Station	BAE	WHB	BID	TEL	p_{ANOVA}
Temperature (°C)	1.5 ± 0.0	1.0 ± 0.0	1.1 ± 0.0	0.7 ± 0.0	-
Salinity (PSU)	33.0 ± 0.5 [a]	32.9 ± 0.1 [a]	32.0 ± 0.0 [b]	32.3 ± 0.3 [b]	**$<10^{-3}$**
pH_T	8.04 ± 0.01 [b]	8.13 ± 0.02 [a]	7.77 ± 0.03 [c]	7.83 ± 0.04 [c]	**$<10^{-3}$**
TA ($\mu molkg^{-1}$)	2298 ± 88 [b]	2442 ± 74 [b]	2399 ± 103 [b]	2839 ± 326 [a]	**0.028**
DIC (mM)	2.28 ± 0.12 [b,c]	2.76 ± 0.30 [a,b]	2.13 ± 0.12 [c]	2.81 ± 0.15 [a]	**0.005**
pCO_2 (µatm)	415 ± 12 [b]	404 ± 33 [b]	722 ± 63 [a]	829 ± 90 [a]	**$<10^{-3}$**

HCO_3^- (μmolkg^{-1})	2154 ± 109	b,c	2590 ± 282	a,b	2035 ± 114	c	2688 ± 143	a	**0.005**
CO_3^{2-} (μmolkg^{-1})	98 ± 9	b	141 ± 20	a	48 ± 4	c	72 ± 7	b,c	**<10^{-3}**
$\Omega_{calcite} = \Omega_{Ca}$	2.36 ± 0.20	b	3.41 ± 0.49	a	1.16 ± 0.09	c	1.75 ± 0.18	b,c	**<10^{-3}**
$\Omega_{aragonite} = \Omega_{Ar}$	1.48 ± 0.13	b	2.14 ± 0.31	a	0.73 ± 0.06	c	1.10 ± 0.11	b,c	**<10^{-3}**

Table 2. Metals concentrations in the sediment (total fraction) at the four stations of Deception Island (West Antarctic Peninsula) on the day of organism sampling (Mean ± SD, n=3). Means sharing the same superscript are not significantly different (α < 0.05).

Total fraction									
	BAE		WHB		BID		TEL		p_{ANOVA}
[Cd] (μg g^{-1})	0.06 ± 0.01	a,b	0.12 ± 0.03	a	0.06 ± 0.02	a,b	0.04 ± 0.01	b	**0.048**
[Cu] (μg g^{-1})	6.74 ± 0.02	a,b	9.33 ± 0.93	a	6.67 ± 0.97	a,b	5.16 ± 0.20	b	**0.029**
[Fe] (μg g^{-1})	9760 ± 1682	b	15814 ± 581	a	10271 ± 1091	b	11277 ± 1711	b	**0.008**
[Pb](μg g^{-1})	0.53 ± 0.10	b	1.13 ± 0.14	a	0.67 ± 0.03	b	0.74 ± 0.20	a,b	**0.011**
[Zn] (μg g^{-1})	29.14 ± 0.24	b	40.57 ± 1.74	a	30.17 ± 2.56	b	28.67 ± 2.89	b	**0.001**

8.1. Table 3. Acid-base physiology of the coelomic fluid and size of *Odontaster validus* and *Sterechinus neumayeri* from the four stations of Deception Island (Mean ± SD, n=6 except TA: n=3). pCO_2, [HCO_3^-], [CO_3^{2-}], values of $\Omega_{calcite}$ and $\Omega_{aragonite}$ were calculated using CO2SYS software with pH_T and DIC values. Means sharing the same superscript are not significantly different (α= 0.05).* Tukey test not significant (p≥0.057)

Odontaster validus									
Station	BAE		WHB		BID		TEL		p_{ANOVA}
pH_T	7.68 ± 0.11		7.77 ± 0.08		7.65 ± 0.08		7.74 ± 0.06		0.080
TA (μmolkg^{-1})	2641 ± 322.46		3054 ± 217		2566 ± 263		3253 ± 834		0.064
DIC (mM)	2.63 ± 0.32		3.02 ± 0.23		2.57 ± 0.28		3.23 ± 0.85		0.090
pCO_2 (μatm)	1129 ± 325.05		1056 ± 217		1205 ± 372		1208 ± 450		0.858
HCO_3^- (μmolkg^{-1})	2512 ± 301.90		2887 ± 218		2457 ± 266		3090 ± 814		0.086
CO_3^{2-} (μmolkg^{-1})	52 ± 16	a,b	69 ± 13	a	43 ± 6	b	67 ± 12	a	**0.004**
$\Omega_{calcite} = \Omega_{Ca}$	1.24 ± 0.39	a,b	1.67 ± 0.31	a	1.05 ± 0.15	b	1.62 ± 0.30	a	**0.005**
$\Omega_{aragonite} = \Omega_{Ar}$	0.78 ± 0.24	a,b	1.04 ± 0.20	a	0.66 ± 0.09	b	1.02 ± 0.19	a	**0.004**
Arm length (mm)	48.6 ± 5.1	a,b	54.3 ± 4.7	a	49.9 ± 5.0	a	46.0 ± 2.5	b	**0.031**
Sterechinus neumayeri									
Station	BAE		WHB		BID		TEL		p_{ANOVA}
pH_T	7.80 ± 0.08	a,b	7.92 ± 0.05	a	7.69 ± 0.12	b	7.72 ± 0.13	b	**0.003**
TA (μmolkg^{-1})	4045 ± 360	b	6095 ± 714	a	4617 ± 946	a,b	5539 ± 1277	a,b	**0.003**
DIC (mM)	3.99 ± 0.35	b	5.85 ± 0.66	a	4.63 ± 0.98	a,b	5.54 ± 1.28	a	**0.015**
pCO_2 (μatm)	1274 ± 235	*	1418 ± 163	*	2005 ± 820	*	2209 ± 809	*	**0.035**
HCO_3^- (μmolkg^{-1})	3810 ± 332	b	5668 ± 650	a	4421 ± 936	a,b	5286 ± 1225	a	**0.005**
CO_3^{2-} (μmolkg^{-1})	102 ± 22.28	b	195 ± 36	a	87 ± 21	b	114 ± 42	b	**<10^{-3}**
$\Omega_{calcite} = \Omega_{Ca}$	2.47 ± 0.54	b	4.70 ± 0.87	a	2.10 ± 0.50	b	2.76 ± 1.02	b	**<10^{-3}**
$\Omega_{aragonite} = \Omega_{Ar}$	1.55 ± 0.34	b	2.94 ± 0.54	a	1.31 ± 0.31	b	1.73 ± 0.64	b	**<10^{-3}**
D test (mm)	40.7 ± 1.6		37.8 ± 6.4		39.3 ± 3.4		40.3 ± 1.3		0.286
H test (mm)	23.8 ± 1.4		20.7 ± 0.6		23.8 ± 1.2		23.1 ± 1.9		0.151

Table 4. Morphometrical (effective length: L_e, height: H, second moment of inertia: I_2) properties of the ambulacral plates of *Odontaster validus* and the ambital plates of *Sterechinus neumayeri*, at the four stations of Deception Island (Mean ± SD, n=6). Means sharing the same superscript are not significantly different (α= 0.05). * Tukey test not significant (p ≥0.084)

Odontaster validus					
Station	BAE	WHB	BID	TEL	p_{ANOVA}
L_e (10^{-3} m)	3.09 ± 0.31	3.12 ± 0.24	3.03 ± 0.16	2.80 ± 0.37	0.204
H (10^{-3} m)	0.54 ± 0.07 [a,b]	0.58 ± 0.06 [a,b]	0.63 ± 0.07 [a]	0.49 ± 0.08 [b]	**0.013**
I_2 (10^{-15} m^4)	5.00 ± 1.85 [b]	7.44 ± 1.48 [a,b]	7.92 ± 1.71 [a]	7.14 ± 1.96 [a,b]	**0.038**
Sterechinus neumayeri					
Station	BAE	WHB	BID	TEL	p_{ANOVA}
L_e (10^{-3} m)	6.82 ± 0.16	6.16 ± 0.55	6.48 ± 0.11	6.67 ± 0.69	0.746
H (10^{-3} m)	0.38 ± 0.03	0.33 ± 0.03	0.38 ± 0.04	0.34 ± 0.04	0.193
I_2 (10^{-15} m^4)	2.39 ± 1.02	2.30 ± 1.12	2.16 ± 0.71	2.15 ± 0.65	0.710

Table 5. Characteristic stress (σ_0), Weibull modulus (m: slope of the linearized Weibull curve), characteristic force at fracture (F_{max0}) and characteristic Young's modulus (E_0) of the ambulacral plates of *Odontaster validus* and the ambital plates of *Sterechinus neumayeri* at the four stations of Deception Island, and their respective 95% confidence intervals (CI 95% ± : lower and upper limits of 95% confidence interval). Characteristic values sharing the same superscript are not significantly different based on their respective CI 95.

	Odontaster validus			*Sterechinus neumayeri*		
Station	σ_0 (MPa)	CI 95 -	CI 95 +	σ_0 (MPa)	CI 95 -	CI 95 +
BAE	0.26 [a,b]	0.18	0.39	4.51	3.35	6.08
WHB	0.27 [a]	0.21	0.35	3.78	2.88	4.97
BID	0.14 [b]	0.10	0.20	4.61	3.24	6.56
TEL	0.17 [a,b]	0.12	0.23	4.56	3.05	6.83
Station	m	CI95% -	CI95% +	m	CI95% -	CI95% +
BAE	0.99	0.68	1.45	1.51	0.98	2.35
WHB	1.49	1.02	2.18	1.42	0.97	2.06
BID	1.17	0.80	1.72	1.10	0.75	1.59
TEL	1.22	0.84	1.79	0.99	0.67	1.46
Station	F_{max0} (N)	CI95% -	CI95% +	F_{max0} (N)	CI95% -	CI95% +
BAE	1.46 [b,c]	1.17	1.83	0.76 [a]	0.63	0.93
WHB	2.32 [a]	1.98	2.72	0.76 [a]	0.64	0.90
BID	1.35 [c]	1.12	1.63	0.69 [a,b]	0.54	0.89
TEL	1.99 [a,b]	1.68	2.35	0.48 [b]	0.40	0.58
Station	E_0(GPa)	CI95% -	CI95% +	E_0(GPa)	CI95% -	CI95% +
BAE	0.93 [a]	0.66	1.30	0.11	0.08	0.16
WHB	0.73 [a,b]	0.55	0.97	0.09	0.06	0.12
BID	0.41 [b]	0.29	0.57	0.12	0.08	0.17
TEL	0.52 [a,b]	0.39	0.70	0.13	0.09	0.21

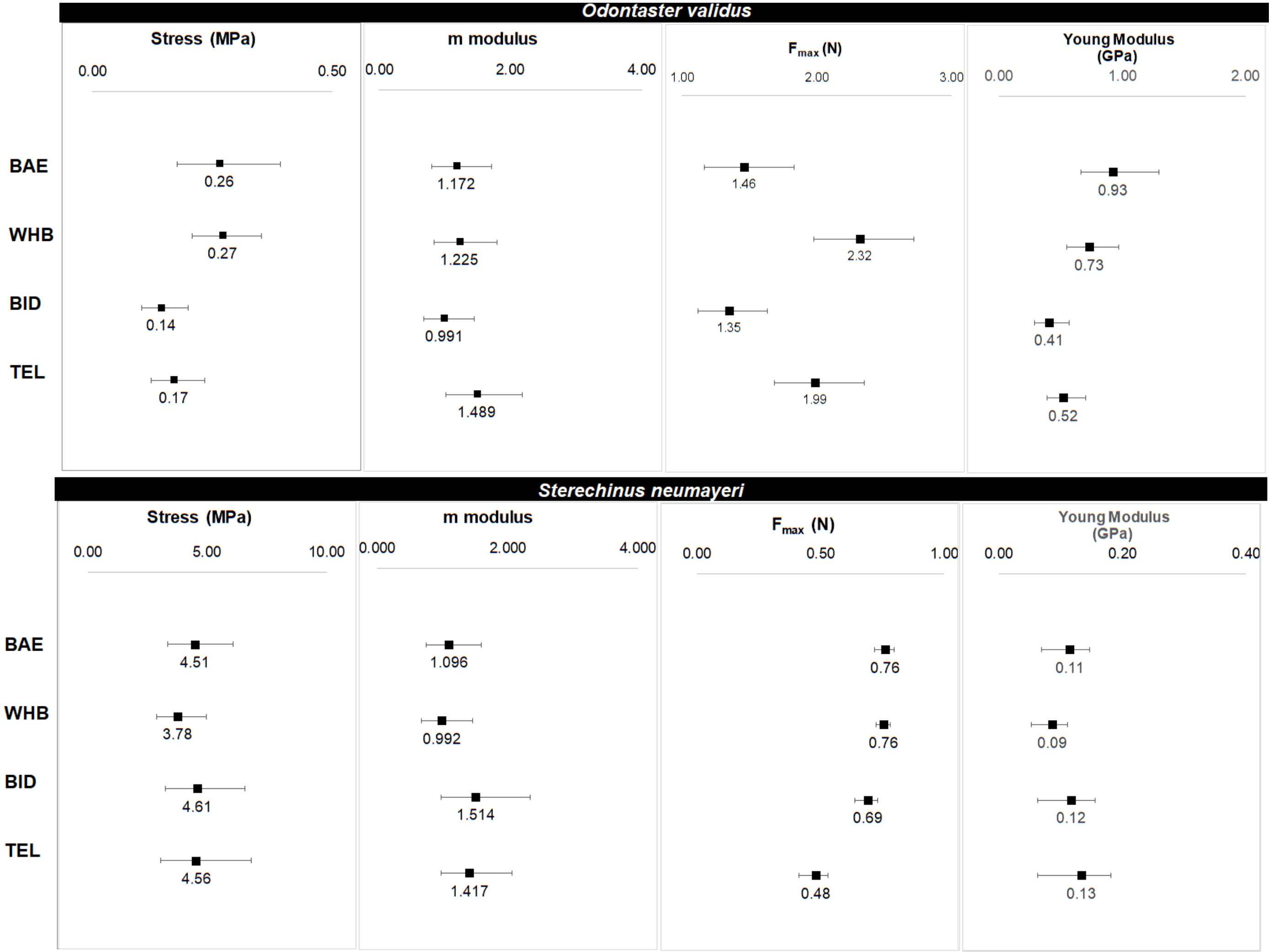

<u>Figure 2. </u>: Characteristic mechanical properties: stress, Weibull modulus, F_{max} and Young's modulus (E), value at which 63% of the plates break) with lower and upper 95% confidence intervals (CI) of ambulacral plates of *Odontaster validus* and interambulacral ambital plates of *Sterechinus neumayri* at the four station of Deception Island.

Table 6. Metals concentrations (Cd, Cu, Fe, Pb and Zn) in different body parts of the sea star *Odontaster validus* (integument, gonads and pyloric caeca) and of the sea urchin *Sterechinus neumayeri* (integument, gonads and digestive tract) from the four stations at Deception Island (Mean ± SD, n=6).

Odontaster validus					
		BAE	WHB	BID	TEL
Integument	[Cd] (µgg^{-1})	89.10 ± 39.85	170.85 ± 33.86	142.75 ± 10.69	89.54 ± 36.95
	[Cu] (µgg^{-1})	13.59 ± 6.81	13.96 ± 3.61	29.92 ± 12.04	13.09 ± 3.33
	[Fe] (µgg^{-1})	346.38 ± 88.27	221.60 ± 41.09	293.45 ± 88.93	295.44 ± 235.83
	[Pb] (µgg^{-1})	0.60 ± 0.28	0.45 ± 0.10	1.10 ± 0.35	0.56 ± 0.30
	[Zn] (µgg^{-1})	75.47 ± 4.36	61.26 ± 6.01	74.07 ± 6.19	74.53 ± 9.50
		BAE	WHB	BID	TEL
Gonads	[Cd] (µgg^{-1})	30.64 6.29	6.59 ± 2.06	21.74 ± 7.75	12.65 ± 5.29
	[Cu] (µgg^{-1})	6.61 ± 7.75	3.08 ± 0.66	3.60 ± 2.09	2.70 ± 0.91
	[Fe] (µgg^{-1})	322.22 ± 65.81	265.04 ± 123.82	291.50 ± 131.14	113.05 ± 25.79
	[Pb] (µgg^{-1})	0.56 ± 0.41	0.22 ± 0.02	0.71 ± 0.34	0.29 ± 0.19
	[Zn] (µgg^{-1})	99.17 ± 5.16	80.33 ± 2.27	100.75 ± 10.43	94.53 ± 6.98
		BAE	WHB	BID	TEL
Pyloric caeca	[Cd] (µgg^{-1})	16.80 10.04	9.79 ± 0.89	20.71 ± 10.83	8.96 ± 2.37
	[Cu] (µgg^{-1})	24.20 ± 10.83	17.27 ± 2.81	30.01 ± 9.17	17.55 ± 2.87
	[Fe] (µgg^{-1})	6916.31 ± 2462.77	9651.78 ± 1685.48	2229.30 ± 508.01	662.73 ± 157.91
	[Pb] (µgg^{-1})	0.31 ± 0.15	0.27 ± 0.04	0.94 ± 0.54	0.28 ± 0.16
	[Zn] (µgg^{-1})	386.85 ± 97.11	94.07 ± 25.39	371.02 ± 91.48	414.33 ± 50.72

Sterechinus neumayeri					
		BAE	WHB	BID	TEL
Integument	[Cd] (µgg^{-1})	1.20 ± 0.31	1.46 ± 0.21	1.50 ± 0.24	1.39 ± 0.24
	[Cu] (µgg^{-1})	1.12 ± 0.24	0.73 ± 0.16	1.63 ± 0.49	2.43 ± 0.76
	[Fe] (µgg^{-1})	290.97 ± 45.96	140.39 ± 35.44	350.42 ± 77.55	589.78 ± 218.65
	[Pb] (µgg^{-1})	0.55 ± 0.11	0.18 ± 0.06	0.55 ± 0.32	0.55 ± 0.28
	[Zn] (µgg^{-1})	401.90 ± 153.96	407.46 ± 119.21	332.90 ± 81.94	619.86 ± 89.94
		BAE	WHB	BID	TEL
Gonads	[Cd] (µgg^{-1})	1.19 0.51	1.71 ± 1.08	2.07 ± 1.32	1.54 ± 0.40
	[Cu] (µgg^{-1})	1.87 ± 1.32	2.01 ± 0.35	1.52 ± 0.25	1.35 ± 0.51
	[Fe] (µgg^{-1})	284.25 ± 168.36	727.45 ± 404.33	446.21 ± 218.21	509.03 ± 344.45
	[Pb] (µgg^{-1})	0.55 ± 0.19	0.20 ± 0.06	0.55 ± 0.36	0.55 ± 0.49
	[Zn] (µgg^{-1})	127.87 ± 23.33	112.78 ± 44.41	120.89 ± 33.71	135.98 ± 25.24
		BAE	WHB	BID	TEL
Digestive tract	[Cd] (µgg^{-1})	6.06 1.22	4.00 ± 0.94	8.15 ± 3.56	1.68 ± 0.59
	[Cu] (µgg^{-1})	4.91 ± 3.56	10.95 ± 7.37	5.66 ± 1.81	3.60 ± 1.55
	[Fe] (µgg^{-1})	1595.45 ± 402.50	6260.74 ± 1322.75	3977.64 ± 1559.87	3009.00 ± 576.63
	[Pb] (µgg^{-1})	0.55 ± 1.10	0.72 ± 0.45	0.55 ± 0.76	0.55 ± 0.03
	[Zn] (µgg^{-1})	216.56 ± 110.95	114.54 ± 21.75	95.58 ± 30.30	84.64 ± 58.23

Table 7. Pearson correlation coefficients and associated probabilities between $pH_{T\text{-}CF}$ and metal concentrations in the different compartments of *Odontaster validus* and *Sterechinus neumayeri*

Odontaster validus						
		Cd	**Cu**	**Fe**	**Pb**	**Zn**
Integument	pH_{CF}	0.249	-0.321	-0,390	-0.299	-0.093
	p-value	0.006	$<10^{-3}$	$<10^{-3}$	0.001	0.314
Gonads	pH_{CF}	-0.458	-0.209	-0.116	-0.139	-0.393
	p-value	0.024	0.326	0.591	0.518	0.057
Pyloric caeca	pH_{CF}	-0.343	-0.294	0.224	-0.157	-0.365
	p-value	0.101	0.164	0.294	0.464	0.079
Sterechinus neumayeri						
Integument	pH_{CF}	-0.358	-0.642	-0.234	-0.312	-0.462
	p-value	$<10^{-3}$	$<10^{-3}$	0.011	0.001	$<10^{-3}$
Gonads	pH_{CF}	-0.287	0.463	0.316	-0.435	-0.525
	p-value	0.175	0.023	0.132	0.034	0.008
Digestive tract	pH_{CF}	-0.261	0.341	0.331	0.098	-0.118
	p-value	0.229	0.112	0.123	0.656	0.591

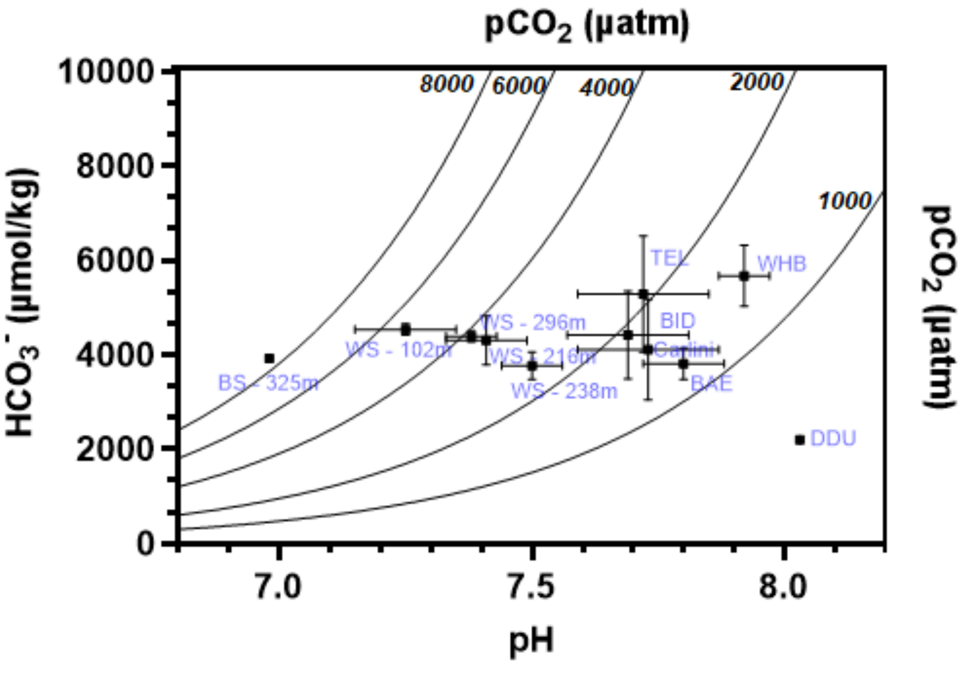

Figure 3. pH-bicarbonate (Davenport) diagram showing differences of acid-base physiology (mean ± SD, n=3) of *Sterechinus neumayeri* at different stations and depths (15 m to 325 m) in Antarctica. BS: Bransfield Strait, WS : Weddel Sea (data from Collard et al. 2015), DDU : Dumont d'Urville (Terre-Adélie, unpublished data from Dubois Ph.), Carlini (King George Island, WAP, unpublished data from Agüera A.) and DI: Deception Island (WAP, present study). The solid curved lines represent pCO_2 isopleths.

Supplementary information

Effects of ocean acidification on acid-base physiology, skeleton properties, and metal contamination in two echinoderms from vent sites in Deception Island, Antarctica

S01. Results of one-way ANOVA (Station: fixed factor) on physico-chemical parameters of the seawater from four stations of Deception Island (West Antarctic Peninsula) (n=3).

	Factor	Sum of squares	Numerator df	Denominator df	Mean square	F-ratio	p_{ANOVA}
Temperature	Station	1.638	3	16	0.546		
	Error	0.000	16		0.000		
Salinity	Station	3.562	3	16	1.187	15.269	
	Error	1.244	16		0.078		
pH_T	Station	0.252	3	8	0.084	118.502	**<10^{-3}**
	Error	0.006	8		0.001		
TA	Station	508625.61	3	8	169541.870	5.216	**0.028**
	Error	260034.798	8		32504.350		
DIC	Station	1.055	3	8	0.352	9.875	**0.005**
	Error	0.285	8		0.036		
pCO_2	Station	419799.586	3	8	1398933.195	41.859	**<10^{-3}**
	Error	26743.772	8		3342.972		
$[HCO_3^-]$	Station	926054.810	3	8	308684.937	9.905	**0.005**
	Error	249304.651	8		31163.081		
$[CO_3^{2-}]$	Station	14342.047	3	8	4780.682	34.216	**<10^{-3}**
	Error	1117.750	8		139.719		
ΩCa	Station	8.315	3	8	2.772	34.303	**<10^{-3}**
	Error	0.646	8		0.081		
ΩAr	Station	3.272	3	8	1.091	34.266	**<10^{-3}**
	Error	0.255	8		0.032		

S02. Results of one-way ANOVA (Station: fixed factor) on metal concentrations (Cd. Cu. Fe. Pb. Zn) of the total fraction from four stations of Deception Island (West Antarctic Peninsula) (n=3).

Total Fraction						
	Factor	Sum of squares	Degree of freedom	Mean square	F-ratio	p_{ANOVA}
Cd	Station	0.009	3	0.004	4.135	**0.048**
	Error	0.006	8	0.001		
Cu	Station	26.961	3	8.987	5.106	**0.029**
	Error	14.081	8	1.760		
Fe	Station	6.86E+07	3	2.29E+07	8.372	**0.008**
	Error	2.19E+07	8	2.73E+06		
Pb	Station	0.591	3	0.197	7.260	**0.011**
	Error	0.217	8	0.027		
Zn	Station	287.846	3	95.949	14.200	**0.001**
	Error	54.056	8	6.757		

S03. Factor loadings plots (left) in all stations pooled and their respective individual loadings plots (right) of principal-component analyses evaluating the relations between metal concentrations in the total fraction sediment and pH_T seawater. n = 6 sampling. % = percentages of observed total variance explained by the factor in the model

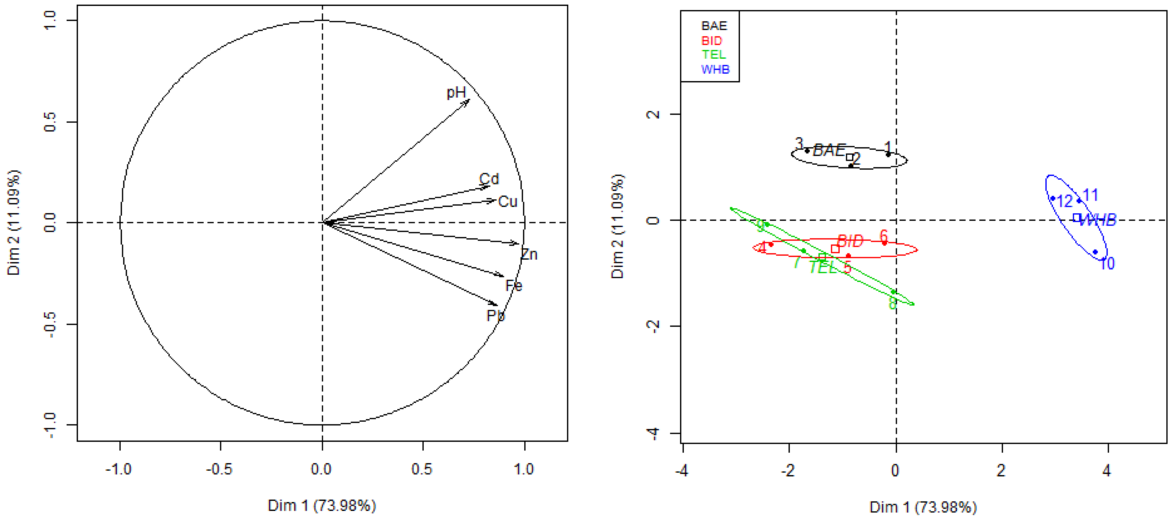

S04. Principal factor analyses description from metal concentrations (Cd. Cu. Fe. Pb. Zn) and pH_e in the total fraction sediment at Deception Island (West Antarctic Peninsula). PC1: first principal component (%). PC2: second principal component (%) and their respective explaining factor (%) Dim. 1: first dimension. Dim. 2: second dimension. ctr: contribution of the variable in the component (%). cos2: squared cosinus of the variable.

Total fraction sediment						
	PC1			**PC2**		
%	**73.979**			**11.085**		
	Dim. 1	ctr	cos2	Dim. 2	ctr	cos2
Cd	0.825	15.326	0.68	0.184	5.097	0.034
Cu	0.857	16.551	0.735	0.114	1.946	0.013
Fe	0.897	18.138	0.805	-0.263	10.394	0.069
Pb	0.863	16.786	0.745	-0.411	25.354	0.169
Zn	0.973	21.318	0.946	-0.103	1.608	0.011
Ph	0.726	11.881	0.527	0.608	55.601	0.37

S05. Results of one-way ANOVA (Station: fixed factor) on physico-chemical parameters of the coelomic fluid and morphometrical of *Odontaster validus* from four stations of Deception Island (West Antarctic Peninsula) (n=3).

(n=3).

	Factor	Sum of squares	Numerator df	Mean square	F-ratio	p_{ANOVA}
pH_T	Station	0.055	3	0.018	2.610	0.080
	Error	0.140	20	0.007		
TA	Station	1.95E+06	3	6.51E+05	2.841	0.064
	Error	4.58E+06	20	2.29E+05		
DIC	Station	1.788	3	0.596	2.487	0.090
	Error	4.795	20	0.240		
pCO_2	Station	9.39E+04	3	3.13E+04	0.254	0.858
	Error	2.47E+06	20	1.23E+05		
$[HCO_3^-]$	Station	1.66E+06	3	5.52E+05	2.535	0.086
	Error	4.36E+06	20	2.18E+05		
$[CO_3^{2-}]$	Station	2796.033	3	923.011	6.004	**0.004**
	Error	3104.389	20	155.219		
ΩCa	Station	1.610	3	0.537	5.934	**0.005**
	Error	1.809	20	0.090		
ΩAr	Station	0.635	3	0.212	5.964	**0.004**
	Error	0.710	20	0.025		
Length arm	Station	216.448	3	72.149	3.620	**0.031**
	Error	398.576	20	19.928		

S06. Results of one-way ANOVA (Station: fixed factor) on physico-chemical parameters of the coelomic fluid and morphometrical of *Sterechinus neumayeri* from four stations of Deception Island (West Antarctic Peninsula) (n=3).

	Factor	Sum of squares	Numerator df	Denominator df	Mean square	F-ratio	p_{ANOVA}

pH_T	Station	0.197	3	20	0.066	6.566	**0.003**
	Error	0.200	20		0.010		
TA	Station	1.52E+07	3	20	5.06E+06	6.389	**0.003**
	Error	1.59E+07	20		7.93E+05		
DIC	Station	11.414	3	18	3.805	4.580	**0.015**
	Error	14.952	18		0.831		
pCO_2	Station	3.66E+06	3	20	1.22E+06	3.470	**0.035**
	Error	7.04E+06	20		3.52E+05		
$[HCO_3^-]$	Station	1.27E+06	3	20	4.23E+06	5.812	**0.005**
	Error	1.45E+07	20		7.27E+05		
$[CO_3^{2-}]$	Station	4.17E+04	3	20	1.39E+04	13.891	**$<10^{-3}$**
	Error	2.00E+04	20		1.00E+03		
ΩCa	Station	24.180	3	20	8.060	13.818	**$<10^{-3}$**
	Error	11.666	20		0.583		
ΩAr	Station	9.511	3	20	3.170	1.854	**$<10^{-3}$**
	Error	4.577	20		0.229		
D	Station	66.065	3	20	22.022	1.352	0.286
	Error	325.850	20		16.293		
H	Station	129.871	3	20	43.290	1.968	0.151
	Error	439.970	20		21.998		

S07. Results of ANOVA model III (station: fixed factor. individual (ind): nested random factor) on morphometrical properties of the ambulacral plates of *Odontaster validus* from four stations of Deception Island (West Antarctic Peninsula) (n=6).

	Factor	Sum of squares	Degree of freedom	Mean square	F-ratio	p_{ANOVA}
L_e	Station	1.97E-06	3	6.57E-07	1.675	0.204
	Ind(Station)	1.00E-05	20	3.99E-07		
	Error	2.00E-05	95	1.95E-07		
H	Station	3.07E-07	3	1.02E-06	4.626	**0.013**
	Ind(Station)	4.42E-07	20	2.21E-08		

	Error	2.38E-06	95	2.50E-08		
I_2	Station	1.44E-28	3	4.79E-29	3.399	**0.038**
	Ind(Station)	2.82E-28	20	1.41E-29		
	Error	1.88E-27	92	2.04E-29		

S08. Results from characteristic mechanical properties and their 95% confidence intervals on ambulacral plates of *Odontaster validus* from four stations of Deception Island (West Antarctic Peninsula) according to Butikofer et al. 2015. mhat ($\hat{m}$) and shat ($\widehat{s}$) are estimates for m (Weibull modulus) and F_{max0}. E_0 an σ_0 (characteristic F_{max}. Young's modulus and strength. respectively). 95% CI $_M$ lower and upper: lower and upper limits of 95% confidence intervals on m (Weibull modulus) value.

F_{max} (N)													
station	n	m	C	R^2	p	F_{max0} (N)	mhat	95% CI_m -	95% CI_m +	shat	F_{max0} (N) $CI_{95\%}$ -	F_{max0} (N) $CI_{95\%}$ +
BAE	30	1.725	-0.655	0.966	$<10^{-3}$	1.46	1.725	1.185	2.510	1.462	1.17	1.83
WHB	30	2.429	-2.046	0.982	$<10^{-3}$	2.32	2.429	1.669	3.535	2.322	1.98	2.72
BID	29	2.079	-0.628	0.966	$<10^{-3}$	1.35	2.079	1.419	3.045	1.353	1.12	1.63
TEL	30	2.324	-1.599	0.987	$<10^{-3}$	1.99	2.324	1.597	3.383	1.989	1.68	2.35

Young's Modulus E (GPa)												
station	n	m	C	R^2	p	E_0(GPa)	mhat	95% CI_m -	95% CI_m +	shat	E_0 (GPa) $CI_{95\%}$ -	E_0 (GPa) $CI_{95\%}$ +
BAE	29	1.173	0.089	0.967	$<10^{-3}$	0.93	1.173	0.801	1.719	0.93	0.66	1.30
WHB	29	1.398	0.432	0.976	$<10^{-3}$	0.73	1.398	0.955	2.048	0.73	0.55	0.97
BID	29	1.169	1.045	0.989	$<10^{-3}$	0.41	1.045	0.798	1.713	0.41	0.29	0.57
TEL	29	1.339	0.867	0.956	$<10^{-3}$	0.52	1.339	0.914	1.961	0.52	0.39	0.70

Stress σ (MPa)												
station	n	m	c	R^2	p	σ_0 (MPa)	mhat	95% CI_m -	95% CI_m +	shat	σ_0 (MPa) CI95% -	σ_0 (MPa) $CI_{95\%}$ +
BAE	29	0.991	1.320	0.983	$<10^{-3}$	0.26	0.991	0.676	1.451	0.20	0.18	0.39
WHB	29	1.489	1.943	0.966	$<10^{-3}$	0.27	1.489	1.017	2.182	0.27	0.21	0.35
BID	29	1.172	2.278	0.985	$<10^{-3}$	0.14	1.172	0.800	1.717	0.14	0.10	0.20
TEL	29	1.225	2.175	0.978	$<10^{-3}$	0.17	1.225	0.836	1.794	0.17	0.12	0.23

S09. Results of ANOVA model III (station: fixed factor. individual (ind): nested random factor) on morphometrical properties of the ambital plates of *Sterechinus neumayeri* from four stations of Deception Island (West Antarctic Peninsula) (n=6).

	Factor	Sum of squares	Degree of freedom	Mean square	F-ratio	p_{ANOVA}
L_e	Station	6.98E-06	3	2.33E-06	0.892	0.463

	Ind(Station)	5.22E-05	20	2.61E-06		
	Error	9.01E-05	93	9.69E-07		
H	Station	7.38E-08	3	2.46E-08	2.752	0.070
	Ind(Station)	1.79E-07	20	8.94E-09		
	Error	6.63E-07	93	7.12E-09		
I_2	Station	9.53E-27	3	3.18E-27	0.085	0.967
	Ind(Station)	7.46E-25	20	3.73E-26		
	Error	2.83E-24	86	3.29E-26		

S10. Results from characteristic mechanical properties and their 95% confidence intervals on ambulacral plates of *Sterechinus neumayeri* from four stations of Deception Island (West Antarctic Peninsula) according to Butikofer et al. 2015. mhat ($\hat{m}$) and shat ($\widehat{s}$) are estimates for m (Weibull modulus) and F_{max0}. E_0 an σ_0 (characteristic F_{max}. Young's modulus and strength. respectively). 95% CI $_M$ lower and upper: lower and upper limits of 95% confidence intervals on m (Weibull modulus) value.

F_{max} (N)												
station	n	m	C	R²	p	F_{max0} (N)	mhat	95% CI_m -	95% CI_m +	shat	F_{max0} (N) $CI_{95\%}$ -	F_{max0} (N) $CI_{95\%}$ +
BAE	27	2.078	0.561	0.967	$<10^{-3}$	0.76	2.08	1.399	3.087	0.764	0.63	0.93
WHB	30	2.293	0.636	0.979	$<10^{-3}$	0.76	2.29	1.575	3.337	0.758	0.64	0.90
BID	30	1.577	0.576	0.945	$<10^{-3}$	0.69	1.58	1.084	2.295	0.125	0.54	0.89
TEL	30	2.007	1.466	0.987	$<10^{-3}$	0.48	2.01	1.379	2.921	0.482	0.40	0.58

Young's Modulus E (GPa)												
station	n	m	C	R^2	p	E_0(GPa)	mhat	95% CI_m -	95% CI_m +	shat	E_0 (GPa) $CI_{95\%}$ -	E_0 (GPa) $CI_{95\%}$ +
BAE	22	1.343	2.909	0.967	$<10^{-3}$	0.11	1.343	0.866	2.081	0.11	0.08	0.16
WHB	29	1.173	2.872	0.994	$<10^{-3}$	0.09	1.173	0.806	1.708	0.09	0.06	0.12
BID	29	0.998	2.137	0.945	$<10^{-3}$	0.12	0.998	0.686	1.453	0.12	0.08	0.17
TEL	27	0.938	1.881	0.974	$<10^{-3}$	0.13	0.938	0.636	1.383	0.13	0.09	0.21

Stress σ (MPa)												
station	n	m	c	R^2	p	σ_0 (MPa)	mhat	95% CI_m -	95% CI_m +	shat	σ_0 (MPa) $CI_{95\%}$ -	σ_0 (MPa) $CI_{95\%}$ +
BAE	22	1.514	-2.280	0.954	$<10^{-3}$	4.511	1.514	0.98	2.346	4.511	3.35	6.08
WHB	29	1.417	-1.885	0.966	$<10^{-3}$	3.780	1.417	0.97	2.063	3.780	2.88	4.97
BID	29	1.096	-1.675	0.980	$<10^{-3}$	4.612	1.096	0.75	1.595	4.612	3.24	6.56
TEL	27	0.992	-1.505	0.953	$<10^{-3}$	4.561	0.992	0.67	1.463	4.561	3.05	6.83

<u>S11</u>. Principal factor analyses description from metal concentrations (Cd. Cu. Fe. Pb. Zn) and pH_e in the compartments of *O. validus* (integument. gonads and pyloric caeca) and *S. neumayeri* (integument. gonads and digestive tract) from all sampled stations pooled (BAE. WHB. BID and TEL) of Deception Island (West Antarctic Peninsula). PC1: first principal component (%). PC2: second principal component (%) and their respective explaining factor (%) Dim. 1: first dimension. Dim. 2: second dimension. ctr: contribution of the variable in the component (%) .cos2: squared cosinus of the variable.

Odontaster validus							***Sterechinus neumayeri***						
	PC1			**PC2**				**PC1**			**PC2**		
Integument													
%	**32.356**			**30.431**			%	**45.66**			**24.632**		
	Dim. 1	ctr	cos2	Dim. 2	ctr	cos2		Dim. 1	ctr	cos2	Dim. 2	ctr	cos2
Cd	-0.675	23.484	0.456	0.669	24.513	0.448	**Cd**	0.278	2.830	0.078	-0.767	39.835	0.589
Cu	0.165	1.396	0.027	0.877	42.133	0.769	**Cu**	0.829	25.096	0.688	0.171	1.983	0.029
Fe	0.631	20.511	0.398	-0.212	2.470	0.045	**Fe**	0.812	24.075	0.660	0.296	5.940	0.088
Pb	0.463	11.049	0.214	0.679	25.285	0.462	**Pb**	0.754	20.747	0.568	-0.287	5.569	0.082
Zn	0.601	18.582	0.361	-0.129	0.905	0.017	**Zn**	0.826	24.918	0.683	0.295	5.885	0.087
pH	-0.696	24.978	0.485	-0.293	4.694	0.086	**pH**	-0.253	2.333	0.064	0.776	40.788	0.603
Gonads													
%	**47.474**			**20.055**			%	**39.544**			**20.299**		
	Dim. 1	ctr	cos2	Dim. 2	ctr	cos2		Dim. 1	ctr	cos2	Dim. 2	ctr	cos2
Cd	0.884	27.406	0.781	0.101	0.849	0.010	**Cd**	-0.489	10.068	0.239	-0.711	41.552	0.506
Cu	0.687	16.593	0.473	0.614	31.332	0.377	**Cu**	0.752	23.818	0.565	-0.010	0.009	0.000
Fe	0.608	12.959	0.369	0.503	21.061	0.253	**Fe**	0.586	14.496	0.344	-0.383	12.050	0.147
Pb	0.648	14.726	0.419	-0.526	22.987	0.277	**Pb**	-0.333	4.674	0.111	0.663	36.043	0.439
Zn	0.745	19.477	0.555	-0.477	18.913	0.228	**Zn**	-0.709	21.159	0.502	0.185	2.820	0.034
pH	-0.502	8.839	0.252	0.242	4.859	0.058	**pH**	0.782	25.784	0.612	0.303	7.526	0.092
Pyloric caeca							**Digestive Tract**						
%	**41.797**			**24.073**			%	**38.106**			**20.468**		
	Dim. 1	ctr	cos2	Dim. 2	ctr	cos2		Dim. 1	ctr	cos2	Dim. 2	ctr	cos2
Cd	0.763	23.231	0.583	0.546	20.650	0.298	**Cd**	0.224	2.190	0.050	0.843	57.818	0.710
Cu	0.731	21.289	0.534	0.602	25.055	0.362	**Cu**	-0.448	8.774	0.201	0.113	1.034	0.013
Fe	-0.610	14.815	0.372	0.636	28.019	0.405	**Fe**	-0.731	23.353	0.534	0.365	10.851	0.133
Pb	0.483	9.286	0.233	-0.049	0.170	0.002	**Pb**	0.692	20.967	0.479	-0.033	0.090	0.001
Zn	0.643	16.491	0.414	-0.608	25.566	0.369	**Zn**	0.851	31.698	0.725	-0.192	3.009	0.037
pH	-0.611	14.889	0.373	0.088	0.540	0.008	**pH**	-0.546	13.018	0.298	-0.578	27.198	0.334

S12. Factor loadings plots in all stations pooled and their respective individual loadings plots of principal-component analyses evaluating the relations between metal concentrations in the integument (A-B). in the gonads (C-D) and in the pyloric caeca (E-F) and coelomic fluid pH of O. *validus* in all stations pooled of Deception Island (West Antarctic Peninsula). n = 6 sampling. % = percentages of observed total variance explained by the factor in the model.

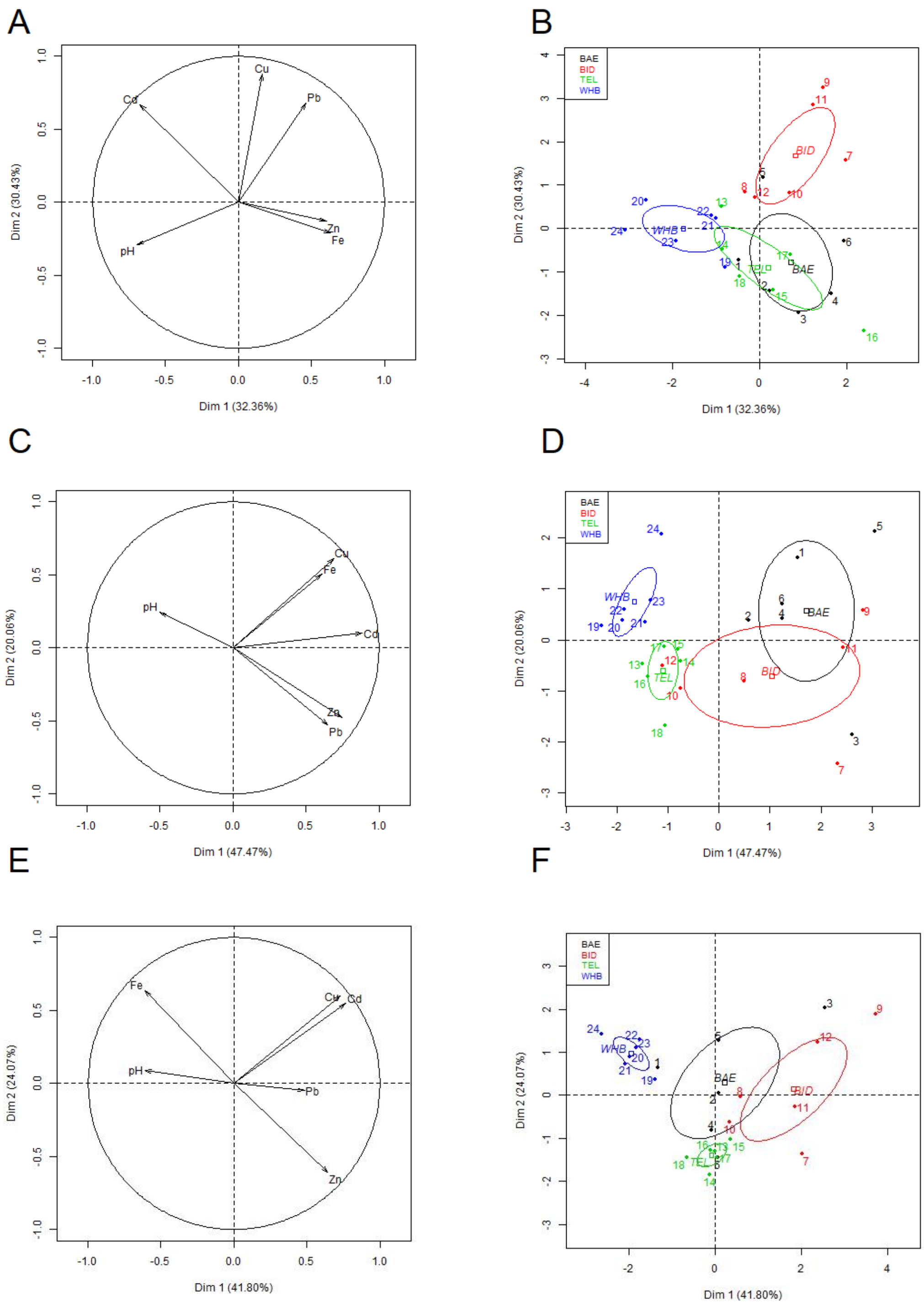

S13. Factor loadings plots and their respective individual loadings plots of principal-component analyses evaluating the relations between metal concentrations in the integument (A-B). in the gonads (C-D) and in the digestive tract (E-F) and coelomic fluid pH of *S. neumayeri* in all stations pooled of Deception Island (West Antarctic Peninsula). n = 6 sampling. % = percentages of observed total variance explained by the factor in the model.

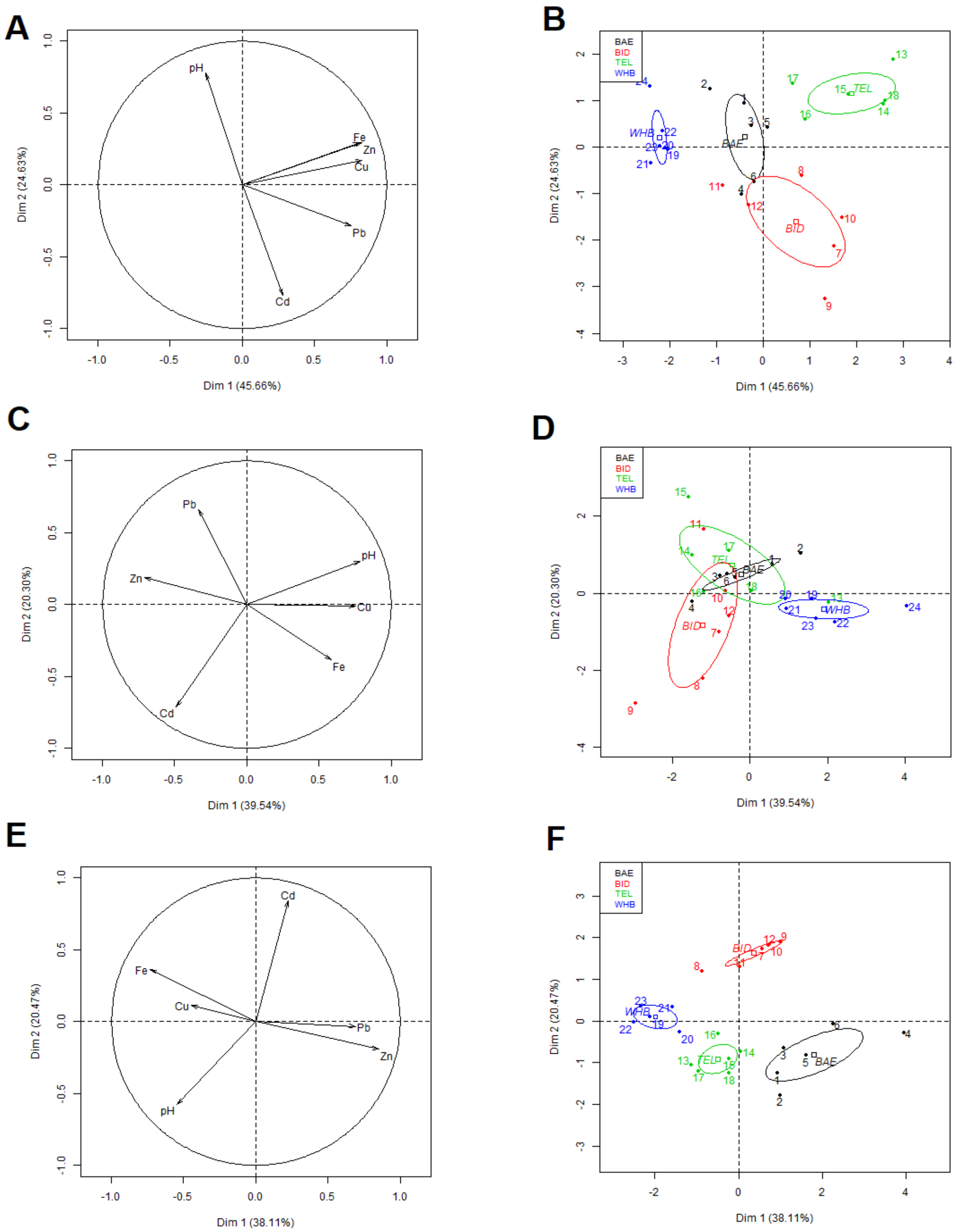

S14. Relationships between pH_{CF}. metal concentrations in the integument and mechanical properties of the skeleton of *Odontaster validus* (GLM following : Considered mechanical variable = a[Cd] + b[Pb] + c[Cu] + d[Fe] +e [Zn] + f pH_{CF} + g [Cd]* pH_{CF} + h [Pb]* pH_{CF} + i [Cu]* pH_{CF} + j [Fe]* pH_{CF} + k [Zn]* pH_{CF} + constant)

FMAX

Regression Coefficients B = $(X'X)^{-1}X'Y$

Effect	Coefficient	Standard Error	Std. Coefficient	Tolerance	t	p-value
CONSTANT	-228.877	133.300	0.000	.	-1.717	0.089
CD	0.331	0.263	21.491	2.525E-005	1.261	0.210
CU	1.013	0.660	14.057	8.749E-005	1.536	0.128
FE	0.184	0.098	35.591	2.046E-005	1.880	0.063
PB	4.846	29.535	2.456	3.271E-005	0.164	0.870
ZN	1.490	1.406	18.117	2.507E-005	1.059	0.292
PH_LC	30.033	17.327	3.668	0.002	1.733	0.086
PH_LC*CD	-0.043	0.034	-21.571	2.474E-005	-1.253	0.213
PH_LC*CU	-0.135	0.086	-14.164	8.919E-005	-1.563	0.121
PH_LC*FE	-0.024	0.013	-35.144	2.088E-005	-1.876	0.063
PH_LC*PB	-0.667	3.849	-2.575	3.315E-005	-0.173	0.863
PH_LC*ZN	-0.195	0.183	-18.297	2.492E-005	-1.067	0.288

Young's modulus E

Regression Coefficients B = $(X'X)^{-1}X'Y$

Effect	Coefficient	Standard Error	Std. Coefficient	Tolerance	t	p-value
CONSTANT	2.901E+011	1.280E+011	0.000	.	2.265	0.026
CD	-5.201E+008	2.534E+008	-38.751	2.413E-005	-2.053	0.043
CU	-4.041E+008	6.282E+008	-6.534	8.335E-005	-0.643	0.521
FE	-1.689E+008	91.894.120.638	-37.907	2.023E-005	-1.838	0.069
PB	5.970E+009	2.862E+010	3.507	3.043E-005	0.209	0.835
ZN	-2.346E+009	1.358E+009	-32.957	2.364E-005	-1.728	0.087
PH_LC	-3.754E+010	1.664E+010	-5.162	0.002	-2.255	0.026
PH_LC*CD	67.488.804.325	32.926.371.151	39.050	2.370E-005	2.050	0.043
PH_LC*CU	51.807.244.304	82.151.285.582	6.341	8.507E-005	0.631	0.530
PH_LC*FE	21.934.578.727	11.932.418.174	37.545	2.062E-005	1.838	0.069
PH_LC*PB	-7.714E+008	3.729E+009	-3.456	3.083E-005	-0.207	0.837
PH_LC*ZN	3.043E+008	1.763E+008	33.081	2.341E-005	1.726	0.087

Stress

Regression Coefficients B = $(X'X)^{-1}X'Y$

Effect	Coefficient	Standard Error	Std. Coefficient	Tolerance	t	p-value
CONSTANT	68.696.340.302	37.432.275.760	0.000	.	1.835	0.069
CD	-126.675.101	75.414.458	-32.556	2.375E-005	-1.680	0.096
CU	3.522.446	185.333.970	0.198	8.183E-005	0.019	0.985
FE	-38.125.113	26.876.319	-29.794	2.022E-005	-1.419	0.159
PB	1.767.318.788	8.374.264.445	3.608	3.053E-005	0.211	0.833
ZN	-590.316.399	397.434.054	-28.540	2.416E-005	-1.485	0.141
PH_LC	-8.883.345.937	4.865.649.711	-4.142	0.002	-1.826	0.071
PH_LC*CD	16.491.933	9.799.410	32.866	2.339E-005	1.683	0.095
PH_LC*CU	-888.517	24.231.275	-0.379	8.355E-005	-0.037	0.971
PH_LC*FE	4.959.073	3.489.870	29.566	2.061E-005	1.421	0.158
PH_LC*PB	-230.196.712	1.090.882.495	-3.585	3.091E-005	-0.211	0.833
PH_LC*ZN	76.511.123	51.600.455	28.704	2.381E-005	1.483	0.141

S15. Relationships between pH_{CF}. metal concentrations in the integument and mechanical properties of the skeleton of *Sterechnius neumayeri* (GLM following : Considered mechanical variable = a[Cd] + b[Pb] + c[Cu] + d[Fe] +e [Zn] + f pH_{CF} + g [Cd]* pH_{CF} + h [Pb]* pH_{CF} + i [Cu]* pH_{CF} + j [Fe]* pH_{CF} + k [Zn]* pH_{CF} + constant)

FMAX						
Regression Coefficients B = $(X'X)^{-1}X'Y$						
Effect	**Coefficient**	**Standard Error**	**Std. Coefficient**	**Tolerance**	**t**	**p-value**
CONSTANT	-2.985	8.574	0.000	.	-0.348	0.728
CD	-0.087	1.473	-0.641	7.130E-005	-0.059	0.953
CU	-0.602	5.273	-1.306	6.368E-005	-0.114	0.909
FE	-0.002	0.034	-1.076	2.425E-005	-0.058	0.954
PB	20.665	21.508	15.084	3.382E-005	0.961	0.339
ZN	-0.026	0.023	-17.337	3.500E-005	-1.123	0.264
PH_LC	0.463	1.089	0.163	0.057	0.425	0.672
PH_LC*CD	0.012	0.189	0.671	7.262E-005	0.063	0.950
PH_LC*CU	0.102	0.690	1.669	6.544E-005	0.148	0.883
PH_LC*FE	1.870E-004	0.004	0.807	2.455E-005	0.044	0.965
PH_LC*PB	-2.664	2.785	-14.965	3.407E-005	-0.957	0.341
PH_LC*ZN	0.003	0.003	17.079	3.612E-005	1.124	0.264
Young's modulus E						
Regression Coefficients B = $(X'X)^{-1}X'Y$						
Effect	**Coefficient**	**Standard Error**	**Std. Coefficient**	**Tolerance**	**t**	**p-value**
CONSTANT	4.876E+009	3.125E+009	0.000	.	1.560	0.122
CD	-1.044E+008	5.419E+008	-2.312	6.477E-005	-0.193	0.848
CU	-1.965E+009	1.870E+009	-12.690	6.394E-005	-1.051	0.296
FE	-284.542.992	11.848.785.659	-0.476	2.376E-005	-0.024	0.981
PB	-2.975E+009	7.570E+009	-6.197	3.752E-005	-0.393	0.695
ZN	3.895.431.605	8.333.521.361	7.725	3.415E-005	0.467	0.641
PH_LC	-6.107E+008	3.966E+008	-0.647	0.053	-1.540	0.127
PH_LC*CD	12.951.800.696	69.642.224.978	2.210	6.607E-005	0.186	0.853
PH_LC*CU	2.554E+008	2.445E+008	12.421	6.596E-005	1.045	0.299
PH_LC*FE	33.892.422	1.504.584.558	0.444	2.405E-005	0.023	0.982
PH_LC*PB	3.770E+008	9.795E+008	6.043	3.784E-005	0.385	0.701
PH_LC*ZN	-499.678.008	1.057.991.652	-7.684	3.524E-005	-0.472	0.638
Stress						
Regression Coefficients B = $(X'X)^{-1}X'Y$						
Effect	**Coefficient**	**Standard Error**	**Std. Coefficient**	**Tolerance**	**t**	**p-value**
CONSTANT	1.862E+008	1.039E+008	0.000	.	1.793	0.076
CD	-12.732.533.947	17.966.811.262	-8.521	6.451E-005	-0.709	0.480
CU	-1.558E+008	61.881.164.358	-30.226	6.472E-005	-2.518	0.013
FE	-126.320.894	404.659.872	-6.388	2.227E-005	-0.312	0.756
PB	2.441E+008	2.529E+008	15.373	3.677E-005	0.965	0.337
ZN	181.051.663	284.119.184	10.854	3.215E-005	0.637	0.525
PH_LC	-23.396.454.591	13.178.412.358	-0.744	0.053	-1.775	0.079
PH_LC*CD	1.621.394.334	2.308.475.235	8.360	6.583E-005	0.702	0.484
PH_LC*CU	20.406.932.023	8.089.430.223	29.818	6.676E-005	2.523	0.013
PH_LC*FE	15.694.797	51.384.006	6.213	2.254E-005	0.305	0.761
PH_LC*PB	-31.874.981.684	32.715.851.251	-15.446	3.711E-005	-0.974	0.332
PH_LC*ZN	-23.267.985	36.056.619	-10.817	3.319E-005	-0.645	0.520

S16. Mechanical properties (F_{max}. Young's modulus (E) and stress (σ)) of proximal ambulacral plates of Asteroids and of ambital plates of Euechinoids measured with the same method (three point bending test) from field studies at different places (mean ± sd. 3 ≤ n ≤ 5).

Asteroids						
Place	**Latitude (°)**	**Species**	**F_{max} (N)**	**Young's modulus (E. Pa)**	**Stress (σ. Pa)**	**Ref.**
Deception Island BAE (WAP)	-62.973	*O. validus*	1.24 ± 0.23	8.95E+08 ± 3.65E+08	2.52E+05 ± 9.77E+04	Present study
Deception Island WHB (WAP)	-62.973	*O. validus*	2.02 ± 0.59	6.63E+08 ± 2.25E+08	2.44E+05 ± 1.04E+05	Present study
Sorfjord Station 4 (Norway)	77.567	*A. rubens*	4.74 ± 0.48	9.03E+09 ± 6.56E+09		(Moureaux *et al.*. 2011)
Kiel Fjord (Baltic Sea)	54.330	*A. rubens*	1.24 ± 0.47	3.09E+09 ± 2.57E+09	4.21E+07 ± 2.43E+07	Di Giglio et al. submitted
Euechinoids						
Place	**Latitude**	**Species**	**Fmax (N)**	**Young's modulus (E. Pa)**	**Stress (σ. Pa)**	**Ref.**
Deception Island BAE (WAP)	-62.973	*S. neumayeri*	0.66 ± 0.22	9.20E+07 ± 4.53E+07	3.67E+06 ± 2.11E+06	Present study
Deception Island WHB (WAP)	-62.973	*S. neumayeri*	0.67 ± 0.22	7.92E+07 ± 4.90E+07	3.42E+06 ± 2.11E+06	Present study
Vulcano CO_2 vent (Italy)	38.426	*P. lividus*	5.96 ± 1.71	4.18E+10 ± 1.49E+10	3.84E+08 ± 1.94E+08	Di Giglio et al. submitted
Intertidal pools Crozon (France)	48.246	*P. lividus*	9.60 ± 3.80	9.10E+09 ± 6.10E+09		(Collard *et al.*. 2016)
Vulcano CO_2 vent (Itlay)	38.426	*A. lixula*	6.69 ± 1.83	5.18E+10 ± 1.86E+10	4.98E+08 ± 2.02E+08	(Di Giglio *et al.*. 2020)
La Réunion Island (France. Indian Ocean)	-44.297	*Echinometra sp. B*	19.55 ± 4.18	1.24E+09 ± 6.63E+08	2.78E+07 ± 3.15E+07	Di Giglio et al. Unpublished data
Upa-Upasina Reef (Papua New Guinea)	-9.800	*Echinometra sp. C*	22.20 ± 5.33	1.64E+09 ± 1.24E+09	2.48E+07 ± 2.23E+07	Di Giglio et al. Unpublished data
Great Barrier Reef (Australia)	-18.521	*T. gratilla*	12.25 ± 4.05	2.78E+09 ± 1.66E+09	7.98E+07 ± 2.75E+07	Di Giglio et al. Unpublished data
Sydney (Australia)	-33.867	*T. gratilla*	2.59 ± 4.18	9.32E+08 ± 1.10E+09	7.33E+07 ± 7.91E+06	Di Giglio et al. Unpublished data